Appendix A to Managed wetlands for climate action: potential greenhouse gas and subsidence mitigation in the Sacramento-San Joaquin Delta

Scenario development

Lydia J. S. Vaughn[1], Steven J. Deverel[2], Stephanie Panlasigui[1], Judith Z. Drexler[3], Marc A. Olds[2], Jose T. Diaz[2], Kendall Harris[1], James Morris[4], J. Letitia Grenier[1], April Robinson[1], Donna Ball[1]

[1]San Francisco Estuary Institute-Aquatic Science Center
[2]Hydrofocus, Inc.
[3]U.S. Geological Survey, California Water Science Center
[4]University of South Carolina

The analysis extent for *Historical*, *Modern*, and all future scenarios (*Reference*, *GHG 1*, *GHG 2*, and *GHG-habitat*) was defined as the historical extent of tidal wetlands within the legal Delta (Fig. A1).

Figure A1. Analysis extent for scenario modeling.

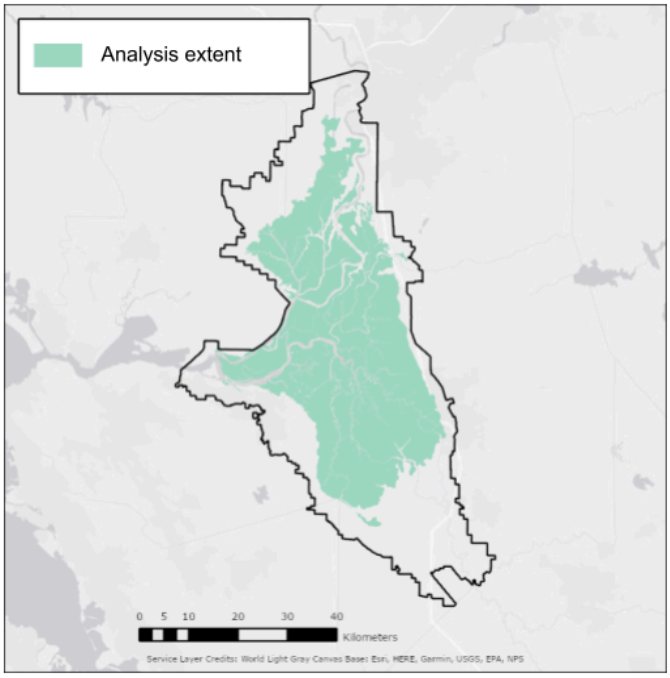

Historical, *Modern*, and *Reference* scenarios were based on historical land cover mapping from Whipple et al. (2012) and modern land cover mapping developed for the Landscape Scenario Planning Tool (LSPT; https://www.sfei.org/projects/landscape-scenario-planning-tool) from 2016 fine-scale vegetation mapping from CDFW VegCAMP (CDFW 2019), and 2016 crop mapping from LandIQ (CDWR and LandIQ 2020). To develop the *Maximum potential* scenario, we first erased areas that were classified as urban or barren. Of the remaining area, everywhere currently within intertidal elevations was assigned to tidal wetland. Subsided areas, defined as below mean lower low water (MLLW) according to a 2017 tidally referenced DEM (DSC 2022b; SFEI 2022), were assigned to be nontidal peat-building wetland managed for subsidence reversal (Fig. A2).

The remaining three scenarios were based on results of the *Maximum potential* and *Reference* scenarios (Fig. A2). To develop the *GHG-habitat* scenario, we first excluded areas that were classified as developed, existing wetland, or cultivated for rice by the LandIQ 2018 dataset of agricultural parcels (CDWR and LandIQ 2021). We selected LandIQ parcels that are currently within the intertidal zone for conversion to tidal marsh. This area included only 12,756 ha, short of the 13,200 ha (32,500 acres) of tidal marsh called for in the Delta Plan Performance Measure 4.16 from the amended chapter 4, “Protect, Restore, and Enhance the Delta Ecosystem” (DSC 2022a). Suisun Marsh offers additional opportunities to meet Delta Plan tidal restoration targets, but was not included in this study’s analysis area. In addition to this 12,756 ha of tidal wetland, the *GHG-habitat* scenario included 12,165 ha of managed wetland for subsidence reversal and carbon sequestration (Delta Plan Performance Measure 5.2; DSC 2013). From the *Maximum potential* scenario, we identified all parcels converted to nontidal wetland in which the median elevation was predicted to reach an elevation within -90 cm relative to mean tide level (MTL; the lowest elevation band used in CWEM modeling) within the 40-year modeling period (2017-2057). These parcels were ranked by potential GHG emissions reduction, and the highest ranked fields were assigned to be nontidal peat-building wetland managed for subsidence reversal until the total area surpassed the 1,400 ha (3,500 acres) of subsidence reversal for tidal reconnection required by the Delta Plan Performance Measure 4.12 (DSC 2022a). We ranked all remaining parcels according to potential GHG emissions reduction and assigned rice to the highest-ranked parcels until the total area surpassed 45% of the total managed nontidal wetland target. Lastly, we continued assigning nontidal wetland to parcels on the basis of GHG emissions reduction until the total area of managed nontidal wetland surpassed 12,100 ha.

To develop landscape configurations for *GHG 1* and *GHG 2*, we first excluded areas that were classified as developed, existing wetland, or cultivated for rice and assigned LandIQ parcels to be nontidal peat-building wetland or rice field on the basis of highest rank for potential GHG benefit for a total of 30,972 ha (76,500 acres) for *GHG 1* and 15,425 ha (38,100 acres) for *GHG 2*. For each scenario, the first 45% of parcel acreage was assigned to rice and the remaining parcels were assigned to nontidal peat-building wetland.

Figure A2. Land use conversions modeled in future scenarios for the Sacramento-San Joaquin Delta. For each of the four future scenarios that include land use conversions, the map shows the placement of rice fields, nontidal peat-building wetland managed for subsidence reversal, and tidal wetland according to potential GHG emissions reduction and elevation.

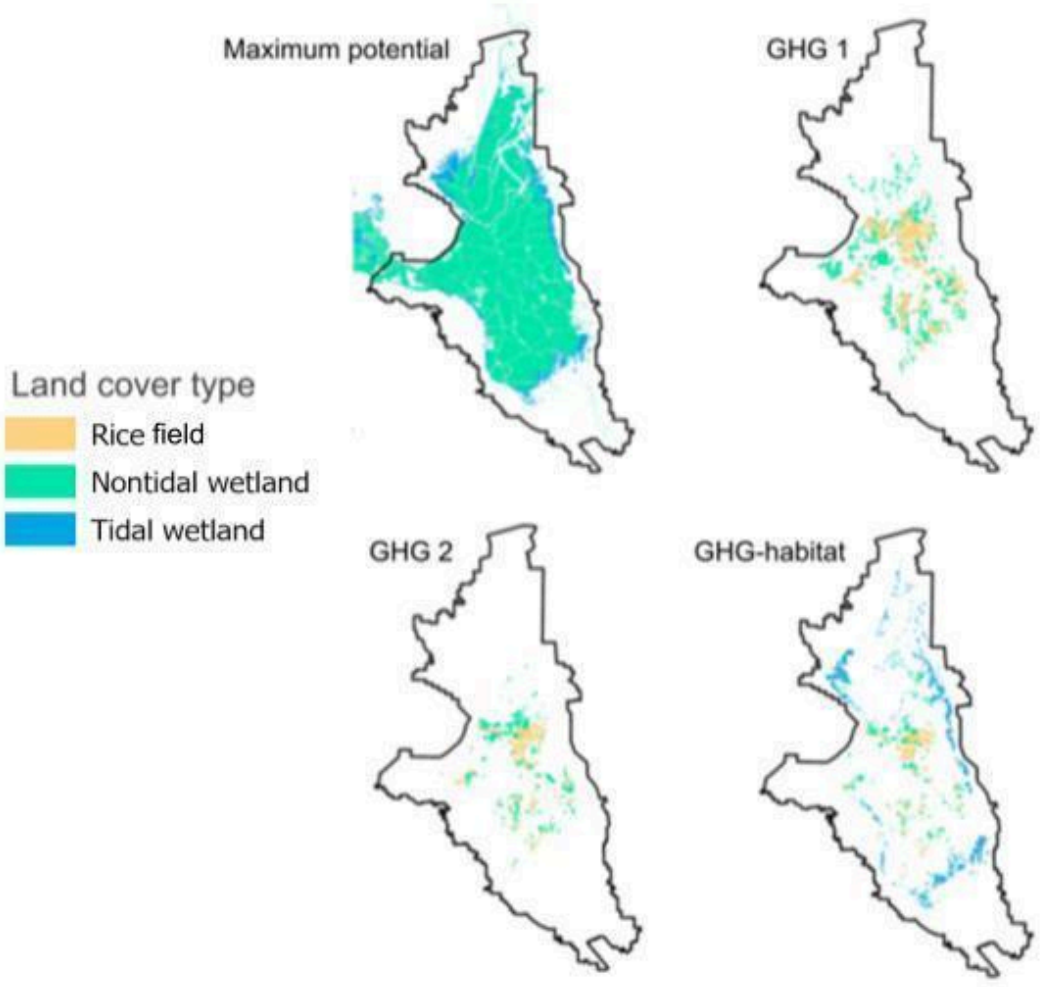

References

[CDFW] California Department of Fish and Wildlife. 2019. Vegetation and Land Use Classification and Map Update of the Sacramento-San Joaquin River Delta. Available from: https://nrm.dfg.ca.gov/FileHandler.ashx?DocumentID=174866&inline

[CDWR and LandIQ] California Department of Water Resources and Land IQ, LLC. 2020. 2016 Statewide Crop Mapping. Available from: https://data.cnra.ca.gov/dataset/statewide-crop-mapping/resource/3b57898b-f013-487a-b472-17f54311edb5

[CDWR and LandIQ] California Department of Water Resources and Land IQ, LLC. 2021. 2018

Statewide Crop Mapping. Available from: https://data.cnra.ca.gov/dataset/statewide-crop-mapping/resource/2dde4303-5c83-4980-a1af-4f321abefe95

[DSC] Delta Stewardship Council. 2022a. Delta Plan Chapter 4. Protect, Restore, and Enhance the Delta Ecosystem. Amended June 2022. Available from: https://deltacouncil.ca.gov/pdf/delta-plan/2022-06-29-chapter-4-protect-restore-and-enhance-the-delta-ecosystem.pdf

[DSC] Delta Stewardship Council. 2022b. Methods Used to Update Ecosystem Restoration Maps Using New Digital Elevation Model and Tidal Data. Appendix Q1 to the Delta Plan Amendments. Available from: https://deltacouncil.ca.gov/pdf/delta-plan/2022-06-29-appendix-q1-methods-used-to-update-ecosystem-restoration-maps-using-new-digital-elevation-model-and-tidal-data.pdf

[SFEI] San Francisco Estuary Institute. 2022. Landscape Scenario Planning Tool User Guide v. 2.0. Available from: https://www.sfei.org/documents/landscape-scenario-planning-tool-user-guide-v20

Whipple A, Grossinger RM, Rankin D, Stanford B, Askevold RA. 2012. Sacramento-San Joaquin Delta historical ecology investigation: exploring pattern and process. SFEI Contribution No. 672. San Francisco Estuary Institute.

Appendix B to Managed wetlands for climate action: potential greenhouse gas and subsidence mitigation in the Sacramento-San Joaquin Delta

Pet carbon quantification

Lydia J. S. Vaughn[1], Steven J. Deverel[2], Stephanie Panlasigui[1], Judith Z. Drexler[3], Marc A. Olds[2], Jose T. Diaz[2], Kendall Harris[1], James Morris[4], J. Letitia Grenier[1], April Robinson[1], Donna Ball[1]

[1]San Francisco Estuary Institute-Aquatic Science Center
[2]Hydrofocus, Inc.
[3]U.S. Geological Survey, California Water Science Center
[4]University of South Carolina

Table A1. Mean peat carbon densities from individual peat profiles, averaged across slices sampled from peat cores. Slices were binned and gap-filled before calculating averages.

(a) *Remnant* peat

Core Profile	**Location**	**Mean organic carbon density (g C cm^{-3})**	**σ organic carbon density (g C cm^{-3})**	**n**	**Reference(s)**
Bacon Channel Island	Bacon Channel Island	0.0388	0.0114	72	Drexler et al. 2009b; Drexler et al. 2009a; Drexler 2011; Drexler et al. 2013; Drexler et al. 2016
Browns Island	Browns Island	0.0464	0.00653	93	Drexler et al. 2009b; Drexler et al. 2009a; Drexler 2011; Drexler et al. 2013; Drexler et al. 2016
Browns Island A High	Browns Island	0.0422	0.0111	5	Callaway et al. 2012
Browns Island B High	Browns Island	0.0435	0.00922	3	Callaway et al. 2012

Franks Wetland	Franks Wetland	0.0335	0.00701	72	Drexler et al. 2009b; Drexler et al. 2009a; Drexler 2011; Drexler et al. 2013; Drexler et al. 2016
Lindsey Slough Marsh Core 1	Lindsey Slough	0.0372	0.00484	5	Drexler et al. 2021
Lindsey Slough Marsh Core 2	Lindsey Slough	0.0308	0.00645	5	Drexler et al. 2021
Middle River Marsh Core 1	Middle River marsh	0.0305	0.00360	5	Drexler et al. 2021
Middle River Marsh Core 2	Middle River marsh	0.0297	0.00456	5	Drexler et al. 2021
Tip of Mandeville Tip Core 3	Tip of Mandeville Tip	0.0362	0.00519	42	Drexler et al. 2009b; Drexler et al. 2009a; Drexler 2011; Drexler et al. 2013; Drexler et al. 2016

(b) *Altered* peat

Profile	**Island**	**Mean organic carbon density (g C cm^{-3})**	**σ organic carbon density (g C cm^{-3})**	**n**	**Altered depth (cm)**	**Reference(s)**
Bacon Island Levee	Bacon Island	0.0741	0.00298	5	37.5	Drexler et al. 2009b; Drexler et al. 2009a; Drexler 2011; Drexler et al. 2013; Drexler et al. 2016
Bacon Island Point C (near center)		0.202	0.0193	9	52.4	Drexler et al. 2009b; Drexler et al. 2009a; Drexler 2011; Drexler et al. 2013; Drexler et al. 2016
Sherman 1	Sherman Island	0.0504	0.00393	8	60	Anthony and Silver 2020
Sherman 2	Sherman Island	0.0662	0.00849	11	60	Anthony and Silver 2020

Twitchell 2	Twitchell Island	0.0586	0.0107	8	60	Anthony and Silver 2020
Twitchell 4	Twitchell Island	0.0359	0.00692	15	80	Craig et al. 2017
Twitchell 6	Twitchell Island	0.0249	0.0152	12	65	Craig et al. 2017
Center of Sherman Island	Sherman Island	0.102	0.0264	23	113.5	Drexler et al. 2009b; Drexler et al. 2009a; Drexler 2011; Drexler et al. 2013; Drexler et al. 2016
Center of Venice Island	Venice Island	0.118	0.0201	17	88	Drexler et al. 2009b; Drexler et al. 2009a; Drexler 2011; Drexler et al. 2013; Drexler et al. 2016
Sherman Island Levee	Sherman Island	0.111	0.0232	12	59	Drexler et al. 2009b; Drexler et al. 2009a; Drexler 2011; Drexler et al. 2013; Drexler et al. 2016
Venice Island Prisoners Point	Venice Island	0.111	0.0136	11	58	Drexler et al. 2009b; Drexler et al. 2009a; Drexler 2011; Drexler et al. 2013; Drexler et al. 2016
Webb Tract Center Island	Webb Tract	0.110	0.0235	18	97	Drexler et al. 2009b; Drexler et al. 2009a; Drexler 2011; Drexler et al. 2013; Drexler et al. 2016
Webb Tract Levee	Webb Tract	0.109	0.0262	21	125	Drexler et al. 2009b; Drexler et al. 2009a; Drexler 2011; Drexler et al. 2013; Drexler et al. 2016

(c) *Deep subsided* peat

Profile	**Island**	**Mean organic carbon**	**σ organic carbon**	**n**	**Reference(s)**

		density (g C cm^{-3})	density (g C cm^{-3})		
Bacon Island Levee	Bacon Island	0.0404	0.00363	19	Drexler et al. 2009b; Drexler et al. 2009a; Drexler 2011; Drexler et al. 2013; Drexler et al. 2016
Bacon Island Point C (near center)	Bacon Island	0.0533	0.00629	10	Drexler et al. 2009b; Drexler et al. 2009a; Drexler 2011; Drexler et al. 2013; Drexler et al. 2016
Center of Sherman Island	Sherman Island	0.0489	0.00888	12	Drexler et al. 2009b; Drexler et al. 2009a; Drexler 2011; Drexler et al. 2013; Drexler et al. 2016
Sherman Island Levee	Sherman Island	0.0395	0.00575	26	Drexler et al. 2009b; Drexler et al. 2009a; Drexler 2011; Drexler et al. 2013; Drexler et al. 2016
Center of Venice Island	Venice Island	0.0463	0.00299	11	Drexler et al. 2009b; Drexler et al. 2009a; Drexler 2011; Drexler et al. 2013; Drexler et al. 2016
Venice Island Prisoners Point	Venice Island	0.0383	0.00843	32	Drexler et al. 2009b; Drexler et al. 2009a; Drexler 2011; Drexler et al. 2013; Drexler et al. 2016
Webb Tract Center Island	Webb Tract	0.0559	0.00639	7	Drexler et al. 2009b; Drexler et al. 2009a; Drexler 2011; Drexler et al. 2013; Drexler et al. 2016
Webb Tract Levee	Webb Tract	0.0481	0.00602	21	Drexler et al. 2009b; Drexler et al. 2009a; Drexler 2011; Drexler et al. 2013; Drexler et al. 2016

With the eight farmed cores spanning *altered* and *deep subsided* categories, we tested whether differences in OC densities from *altered* and *deep subsided* were statistically significant using a linear mixed-effects model with peat class as a fixed effect and core as a random effect. OC density values were log-transformed to meet model assumptions. We found that OC density values differed significantly between the two peat classes ($P << 0.001$). Statistical modeling and significance testing were performed in R version 4.0.2 “Taking Off Again” (R Core Team 2020) using the packages lme4 (Bates et al. 2014) for modeling and lmerTest (Kuznetsova et al. 2014) for significance testing.

Table A2. Summary of linear mixed effects model predicting log-transformed organic carbon density. Peat classes included were *altered* and *deep subsided* peat.

Fixed effect	DF	F value	Pr > F
Peat class	269.08	920.12	< 2.2e-16 ***

Significance. codes: 0 *** 0.001 ** 0.01 * 0.05 0.1

References

Anthony TL, Silver WL. 2020. Mineralogical associations with soil carbon in managed wetland soils. Glob Change Biol. gcb.15309. https://doi.org/10.1111/gcb.15309

Bates D, Maechler M, Bolker BM, Walker S. 2014. lme4: Linear mixed-effects models using Eigen and S4. R package version 1.1-7.

Callaway JC, Borgnis EL, Turner RE, Milan CS. 2012. Carbon Sequestration and Sediment Accretion in San Francisco Bay Tidal Wetlands. Estuaries Coasts. 35:1163–1181. https://doi.org/10.1007/s12237-012-9508-9

Craig MS, Kundariya N, Hayashi K, Srinivas A, Burnham M, Oikawa P. 2017. Geophysical surveying in the Sacramento Delta for earthquake hazard assessment and measurement of peat thickness.

Drexler JZ. 2011. Peat Formation Processes Through the Millennia in Tidal Marshes of the Sacramento–San Joaquin Delta, California, USA. Estuaries Coasts. 34:900. https://doi.org/10.1007/s12237-011-9393-7

Drexler JZ, Alpers CN, Neymark LA, Paces JB, Taylor HE, Fuller CC. 2016. A millennial-scale record of Pb and Hg contamination in peatlands of the Sacramento–San Joaquin Delta of California, USA. Sci Total Environ. 551–552:738–751. https://doi.org/10.1016/j.scitotenv.2016.01.201

Drexler JZ, de Fontaine CS, Brown TA. 2009a. Peat Accretion Histories During the Past 6,000 Years in Marshes of the Sacramento-San Joaquin Delta, CA, USA. Estuaries Coasts Port Repub. 32:871–892. http://dx.doi.org.libproxy.berkeley.edu/10.1007/s12237-009-9202-8

Drexler JZ, Fontaine CS, Deverel SJ. 2009b. The legacy of wetland drainage on the remaining peat in the Sacramento — San Joaquin Delta, California, USA. Wetlands. 29:372–386. https://doi.org/10.1672/08-97.1

Drexler JZ, Khanna S, Lacy JR. 2021. Carbon storage and sediment trapping by Egeria densa Planch., a globally invasive, freshwater macrophyte. Science of the Total Environment. 10;755:142602.

Drexler JZ, Krauss KW, Sasser MC, Fuller CC, Swarzenski CM, Powell A, Swanson KM, Orlando J. 2013. A Long-Term Comparison of Carbon Sequestration Rates in Impounded and Naturally Tidal Freshwater Marshes Along the Lower Waccamaw River, South Carolina. Wetlands. 33:965–974. https://doi.org/10.1007/s13157-013-0456-3

Kuznetsova A, Brockhoff PB, Christensen RHB. 2014. lmerTest: Tests for random and fixed effects for linear mixed effect models (lmer objects of lme4 package).. R package version 2.0-11.

R Core Team. 2020. A language and environment for statistical computing. Vienna, Austria: R Foundation for Statistical Computing. https://www.R-project.org/.

Appendix C to Managed wetlands for climate action: potential greenhouse gas and subsidence mitigation in the Sacramento-San Joaquin Delta

Future modeling approaches and emission factors

Lydia J. S. Vaughn[1], Steven J. Deverel[2], Stephanie Panlasigui[1], Judith Z. Drexler[3], Marc A. Olds[2], Jose T. Diaz[2], Kendall Harris[1], James Morris[4], J. Letitia Grenier[1], April Robinson[1], Donna Ball[1]

[1]San Francisco Estuary Institute-Aquatic Science Center
[2]Hydrofocus, Inc.
[3]U.S. Geological Survey, California Water Science Center
[4]University of South Carolina

Table A3. Overview of modeling approaches and emission factors used in future scenario analyses

Land cover category	Soil type	Peat volume change	CO_2 emissions	CH_4 emissions	N_2O emissions
Tidal wetland (tidal emergent wetland, tidal willow riparian scrub/shrub, and tidal willow thicket)	–	Coastal Wetlands Equilibrium Model (CWEM), C densities from core synthesis	C stock change and CH_4 emissions	11 (5-24) g CH_4 m^{-2} yr^{-1} (Arias-Ortiz et al. 2021)	–
Nontidal peat-building wetland (nontidal emergent wetland below mean lower low water)	–	SEDCALC	SEDCALC	63 (53-73) g CH_4 m^{-2} yr^{-1} (Hemes et al. 2019)	–
Rice field	Organic	–	–	16 (10-22) g CH_4 m^{-2} yr^{-1} (Hemes et al. 2019)	$\ln(\text{kg } N_2O\ m^{-2}\ yr^{-1}) = -0.09 \times \%SOC + 2.59$ (Ye et al. 2016)
Rice field	Mineral	–	-0.04 (0-0.08) kg CO_2 m^{-2} yr^{-1} (Kroodsma and Field 2006)	16 (10-22) g CH_4 m^{-2} yr^{-1} (Hemes et al. 2019)	0.14 (0-0.32) g N_2O m^{-2} yr^{-1} (Verhoeven et al. 2017)
Pasture	Organic	SUBCALC[2]	SUBCALC[2]	8.77 (4.39-13.16) g CH_4 m^{-2} yr^{-1} (IPCC per-head emission rate (Dong et al.	3.7 (1.5-5) g N_2O m^{-2} yr^{-1} (Teh et al. 2011)

				2006) applied to reported stocking densities in Delta pastures)	
Pasture	MIneral	–	-0.04 (0-0.08) kg CO_2 m^{-2} yr^{-1} (Kroodsma and Field 2006)	8.77 (4.39-13.16) g CH_4 m^{-2} yr^{-1} (IPCC per-head emission rate (Dong et al. 2006) applied to reported stocking densities in Delta pastures)	1.79 (0.830-2.75) g N_2O m^{-2} yr^{-1} (Verhoeven et al. 2017)
Cropland	Organic	SUBCALC[2]	SUBCALC[2]	–	kg CO_2e-N_2O = 0.153 (0.043-0.263) x kg CO_2 (Deverel et al. 2017)
Cropland	Mineral	–	-0.04 (0-0.08) kg CO_2 m^{-2} yr^{-1} (Kroodsma and Field 2006)	–	0.33 (0.25-0.41) g N_2O m^{-2} yr^{-1} (De Gryze et al. 2010; Verhoeven et al. 2017)
Grassland	Organic	SUBCALC[2]	SUBCALC[2]	–	kg CO_2e-N_2O = 0.153 (0.043-0.263) x kg CO_2 (Deverel et al. 2017)
Grassland	Mineral	–	0.14 (-0.21-0.49) kg CO_2 m^{-2} yr^{-1} (Ma et al. 2007, grassland sites)	–	–
Seasonal wetland (wet meadow/seasonal wetland)	Organic	SUBCALC[2]	SUBCALC[2]	7.6 (0-15.2) g CH_4 m^{-2} yr^{-1} (Bridgham et al. 2006, freshwater wetlands)	kg CO_2e-N_2O = 0.153 (0.043-0.263) x kg CO_2 (Deverel et al. 2017)
Seasonal wetland (wet meadow/seasonal wetland)	Mineral	–	-0.062 (-0.12-0) kg CO_2 m^{-2} yr^{-1} (Bridgham et al. 2006, freshwater wetlands)	7.6 (0-15.2) g CH_4 m^{-2} yr^{-1} (Bridgham et al. 2006, freshwater wetlands)	–
Oak woodland/savanna	–	–	0.14 (-0.21-0.49) kg CO_2 m^{-2} yr^{-1} (Ma et al. 2007, grassland sites)	–	–
Other wetland (nontidal	–	–	-0.062 (-0.12-0) kg	7.6 (0-15.2) g CH_4	–

emergent wetland at or above mean lower low water, nontidal willow riparian scrub/shrub, nontidal willow thicket, alkali seasonal wetland complex, vernal pool complex, valley foothill riparian)			CO_2 m^{-2} yr^{-1} (Bridgham et al. 2006, freshwater wetlands)	m^{-2} yr^{-1} (Bridgham et al. 2006, freshwater wetlands)	
Urban/barren and open water	–	–	–	–	–

References

Arias-Ortiz A, Wolfe J, Holmquist JR, McNicol G, Needleman B, Stuart-Haentjens EJ, Windham-Myers L, Bridgham SD, Knox S, Megonigal P, Shahan J, Tang J. 2021. A Synthesis of Tidal Wetland Methane Emissions Across the Contiguous United States.

Bridgham SD, Megonigal JP, Keller JK, Bliss NB, Trettin C. 2006. The carbon balance of North American wetlands. 26:29.

De Gryze S, Wolf A, Kaffka SR, Mitchell J, Rolston DE, Temple SR, Lee J, Six J. 2010. Simulating greenhouse gas budgets of four California cropping systems under conventional and alternative management. Ecol Appl. 20:1805–1819.

Deverel S, Jacobs P, Lucero C, Dore S, Kelsey TR. 2017. Implications for Greenhouse Gas Emission Reductions and Economics of a Changing Agricultural Mosaic in the Sacramento–San Joaquin Delta. San Franc Estuary Watershed Sci. [accessed 2021 September 20];15:. https://doi.org/10.15447/sfews.2017v15iss3art2

Dong H, Mangino J, McAllister TA, Hatfield JL, Johnson DE, Lassey KR, Aparecida d Lima M, Romanovskaya A. 2006. IPCC Guidelines for National Greenhouse Gas Inventories, Volume 4, Chapter 10: emissions from livestock and manure management. University Press Cambridge.

Hemes KS, Chamberlain SD, Eichelmann E, Anthony T, Valach A, Kasak K, Szutu D, Verfaillie J, Silver WL, Baldocchi DD. 2019. Assessing the carbon and climate benefit of restoring degraded agricultural peat soils to managed wetlands. Agric For Meteorol. 268:202–214. https://doi.org/10.1016/j.agrformet.2019.01.017

Kroodsma DA, Field CB. 2006. Carbon Sequestration in California Agriculture, 1980–2000. Ecol Appl. 16:1975–1985. https://doi.org/10.1890/1051-0761(2006)016[1975:CSICA]2.0.CO;2

Ma S, Baldocchi DD, Xu L, Hehn T. 2007. Inter-annual variability in carbon dioxide exchange of an oak/grass savanna and open grassland in California. Agric For Meteorol. 147:157–171.

Teh YA, Silver WL, Sonnentag O, Detto M, Kelly M, Baldocchi DD. 2011. Large Greenhouse Gas Emissions from a Temperate Peatland Pasture. Ecosystems. 14:311–325. https://doi.org/10.1007/s10021-011-9411-4

Verhoeven E, Pereira E, Decock C, Garland G, Kennedy T, Suddick E, Horwath W, Six J. 2017. N2O emissions from California farmlands: A review. Calif Agric. 71:148–159. https://doi.org/10.3733/ca.2017a0026

Ye R, Espe MB, Linquist B, Parikh SJ, Doane TA, Horwath WR. 2016. A soil carbon proxy to predict CH4 and N2O emissions from rewetted agricultural peatlands. Agric Ecosyst Environ. 220:64–75.

Appendix D to Managed wetlands for climate action: potential greenhouse gas and subsidence mitigation in the Sacramento-San Joaquin Delta

Modeling of accretion in tidal wetlands with the Coastal Wetlands Equilibrium Model (CWEM)

Lydia J. S. Vaughn[1], Steven J. Deverel[2], Stephanie Panlasigui[1], Judith Z. Drexler[3], Marc A. Olds[2], Jose T. Diaz[2], Kendall Harris[1], James Morris[4], J. Letitia Grenier[1], April Robinson[1], Donna Ball[1]

[1]San Francisco Estuary Institute-Aquatic Science Center
[2]Hydrofocus, Inc.
[3]U.S. Geological Survey, California Water Science Center
[4]University of South Carolina

Key CWEM parameters that vary spatially across the Sacramento-San Joaquin Delta (the Delta) are sea level increase, tidal amplitude, and initial marsh surface elevation. To capture this variation, we ran CWEM for a set of characteristic parameter combinations and applied model results to areas of tidal marsh according to likely parameter values. We defined two characteristic sea level rise (SLR) regions based on modeled future tidal datums from the Delta Stewardship Council's Delta Adapts Climate Change Vulnerability Assessment (DSC 2021a; DSC 2021b). For each 30.5 cm (1 ft) of SLR, this dataset includes predicted tidal datums for 400 discrete points across the Delta and Suisun Marsh. We calculated the change in MSL at each point for 30.5 cm of SLR, and used the natural breaks (jenks) method to create two value categories with maximum differences between the groups (De Smith et al. 2018). The mean change in mean sea level (MSL) of each category was applied to all points, and we then ran an inverse distance weighting interpolation (IDW), which determines raster cell values by averaging the values of neighboring cells, to define regions where SLR is expected to approximately equal the prediction for San Francisco Bay (34 cm by 2060 for our model runs) and where a lower rate of SLR is expected (31 cm, or 90% of the high-SLR increase in MSL) (Fig. A3). Similarly, we calculated tidal amplitude at each location included in the Delta Adapts tidal amplitude dataset, applied the natural breaks method to create three value categories, and then used the IDW interpolation to define three characteristic regions with median tidal amplitudes of 0.48 m, 1.1 m, and 1.6 m.

Figure A3. Modeled tidal amplitude and sea level rise regions for the Sacramento-San Joaquin Delta that were used to scale results of Coastal Wetlands Equilibrium Model analyses to existing and potential areas of tidal marsh. Maps were developed from future tidal datums from the Delta Stewardship Council's Delta Adapts Climate Change Vulnerability Assessment (DSC 2021a; DSC 2021b) using the natural breaks (jenks) method to define characteristic regions. Maps show the median tidal amplitude of defined regions in ft (a) or regions in which MSL is predicted to be 1.1 ft or 90% of 1.1 ft by 2060 (b)

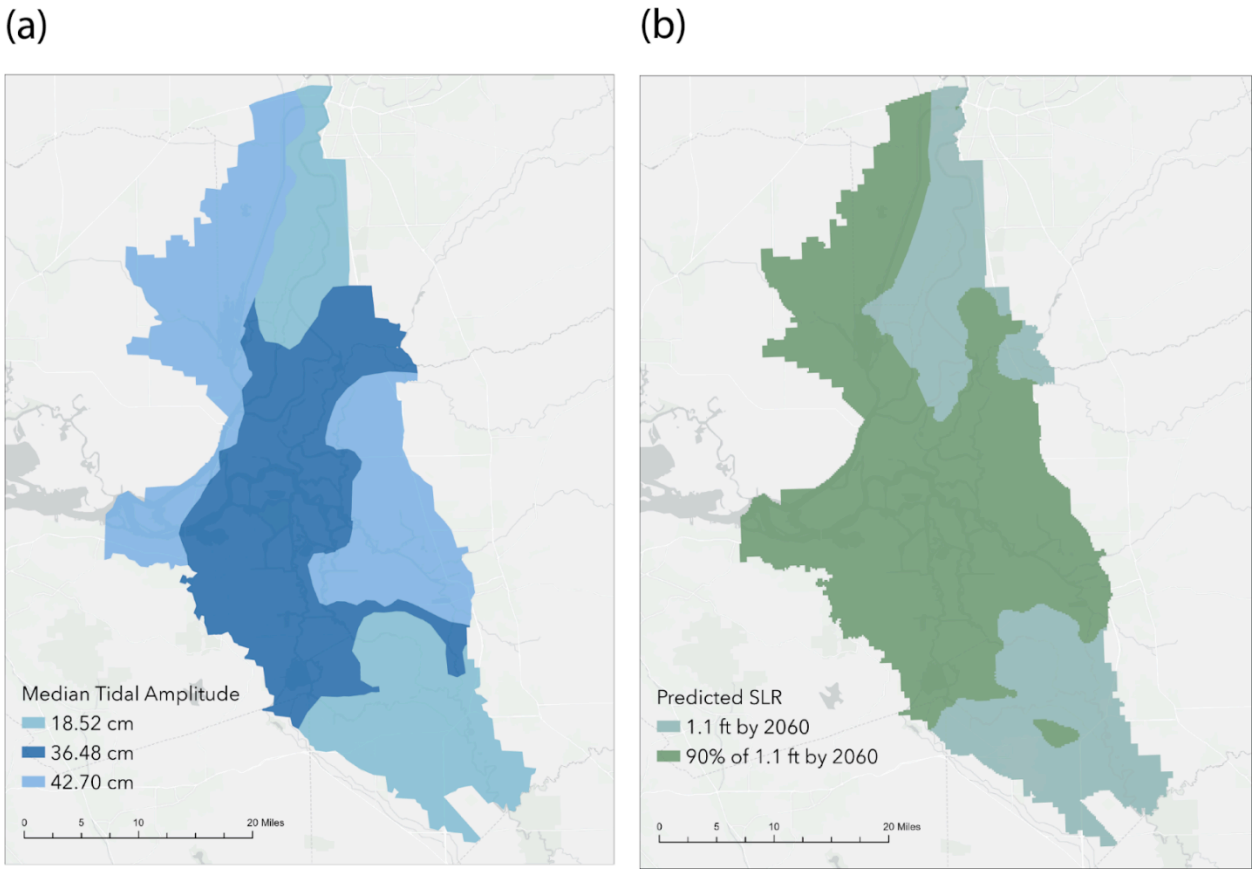

Service layer credits: World Light Gray Canvas Base: Esri, HERE, Garmin, USGS, EPA, NPS

For initial marsh surface elevation, we used a 2017 tidally-referenced digital elevation model (DEM) for the Delta mosaiced from a variety of sources including LiDAR data, existing DEMs, topobathymetric models, and tidal datums derived from a map developed by Siegel and Gillenwater (DSC 2022; SFEI 2022). We defined six elevation bands in which CWEM predicts that vertical accretion will occur, from -97 to +68 cm relative to MSL, with a maximum accretion rate occurring at +10 cm, based on the marsh biomass distributions for Browns Island reported

in Schile et al. (2014), Hester et al. (2016), and Atwater and Hedel (1976). We used the tidally referenced DEM to define marsh surface elevations relative to mean tide level (MTL) (which we used as an approximation for MSL) and binned these elevations into six 30-cm wide elevation bands centered at -90 cm, -60 cm, -30 cm, 0 cm, 30 cm, and 60 cm relative to MTL. To account for vegetation artifacts in the DEM within areas classified as tidal wetland, elevations up to 211 cm MTL were included in the 60 cm band. A complete list of CWEM parameters is provided in Table A4.

Table A4. Parameters values used in Coastal Wetlands Equilibrium Model analysis

Parameter	Value	Units
Sea Level Forecast	23.43, 26.22	cm
Run Time	40	years
Sea Level at Start	126.9	cm (NAVD88)
Starting Sea Level Rise	0.37[1], 0.41[2]	cm/yr
Mean Tidal Amplitude	18.52, 36.48, 42.70	cm
Marsh Elevation @ t0	-90, -60, -30, 0, 30, 60	cm (MSL)
Suspended Mineral Sediment Concentration	20	L
Suspended Organic Sediment Concentration	1	mg/L
Initial Accretion Rate	2.50	mm/yr
Flood Frequency	704	floods per year
Lower Growth Limits	-97	cm rel MSL
Upper Growth Limits	68	cm rel MSL
Optimum Elevation	10	cm rel MSL
Maximum Root Depth	30	cm rel surf
Peak Aboveground Biomass	2500	g/m^2
Below Ground Biomass to Shoot Ratio	2.0	g/g
Below Ground Turnover Rate	0.50	1/year
Time to Maturity	1	years
Organic Matter Decay Rate	0.65	$g\ g^{-1}\ y^{-1}$
Sediment LOI Above-Marsh	30	% of dry wt
Minimum Mineral Input	2	$mg\ cm^{-2}\ yr^{-1}$
Maximum Capture Efficiency	2.80	
Refractory Fraction (kr)	0.13	g/g
Timestep	1.00	years

Carbon Conversion	0.55	g C/g dry wt
Episodic Disturbance1st Occurrence	1	yrs from start
Episodic Disturbance Repeat Interval	1	years
Episodic Disturbance Avg Elevation Gain	0.1	cm

[1]Associated only with the 23.43 cm sea level forecast
[2]Associated only with the 26.22 cm sea level forecast

CWEM was run for all combinations of parameter values (Table A4) for the 40-year period beginning in 2017. The rate of SLR was assumed to increase over time according to a quadratic model, $MSL_t = MSL_0 + at + bt^2$, using a rate of SLR at time 0 of 0.2 cm yr^{-1} to solve for a and b (Nerem et al. 2018; Morris and Renken 2020). For the total sea level increase between 2000 and 2060, we generated an annual SLR timeseries for 2017-2057 for use with CWEM and other scenario modeling (Table A5).

Table A5. Annual increases in mean sea level (MSL) between 2017-2057 used in accretion modeling. Values were derived from polynomial fits for the total sea level rise (SLR) scenario from 2000-2060 (1.1 ft, or 90% of each), with an initial rate of SLR of 0.2 cm yr^{-1}.

Year	Change in MSL relative to 2017, 1.1 ft SLR by 2060 (cm)	Change in MSL relative to 2017, 90% of 1.1 ft SLR by 2060 (cm)
2017	0	0
2018	0.41	0.37
2019	0.83	0.76
2020	1.26	1.15
2021	1.70	1.56
2022	2.16	1.98
2023	2.62	2.40
2024	3.10	2.84
2025	3.59	3.28
2026	4.10	3.74
2027	4.61	4.21

2028	5.14	4.69
2029	5.68	5.17
2030	6.23	5.67
2031	6.80	6.18
2032	7.37	6.70
2033	7.96	7.23
2034	8.56	7.77
2035	9.18	8.32
2036	9.80	8.88
2037	10.44	9.45
2038	11.09	10.03
2039	11.75	10.62
2040	12.42	11.22
2041	13.11	11.83
2042	13.81	12.45
2043	14.52	13.09
2044	15.24	13.73
2045	15.98	14.38
2046	16.72	15.04
2047	17.48	15.72
2048	18.25	16.40
2049	19.03	17.09
2050	19.83	17.80
2051	20.64	18.51
2052	21.46	19.23
2053	22.29	19.97
2054	23.13	20.71
2055	23.99	21.47
2056	24.86	22.24
2057	25.74	23.01

Results from CWEM model runs were used to map predicted scenario vertical accretion according to SLR region, tidal amplitude region, and initial marsh elevation. The six elevation bands, tidal amplitude regions (Fig. A3a), and predicted SLR regions (Fig. A3b) were overlaid in ArcGIS Pro version 2.0 using the union tool, creating a unique layer with new polygons formed by the overlapping boundaries of the joined layers. The Calculate Field tool was used to apply

the vertical accretion rates from CWEM runs to the map in ArcGIS Pro version 3.0 according to tidal amplitude and sea level forecast for 10-, 20-, 30-, and 40-year timeframes. Vertical accretion was converted to carbon accumulation using the carbon density value for *intact* peat derived from the peat core synthesis.

Sea level rise assumptions

The tidal and nontidal accretion models used in this analysis incorporated the Ocean Protection Council (OPC) SLR projection of 1.1 ft by 2060 (the median-probability SLR rate reported by OPC; (OPC 2018). In our scenario modeling, this SLR rate defined the accommodation space available for subsidence reversal in managed wetlands and influenced predicted accretion rates in existing and restored tidal wetlands. Accordingly, using a different rate of SLR in this analysis would alter carbon accumulation and GHG emission rates in nontidal and tidal wetlands. In the case of nontidal wetlands, SLR affects modeled carbon and GHG metrics by defining the timespan over which accretion can occur. For impounded wetlands in shallowly subsided areas, accretion was assumed to stop when the land surface elevation reached 10 cm above MTL, the optimal elevation for emergent marsh biomass in tidal settings in the Delta (Schile et al. 2014). For tidal wetlands, the rate of SLR influences rates of accretion predicted by CWEM in two opposing ways: enhancing vertical accretion in vegetated wetlands and increasing the rate of wetland loss at the lower end of the elevation range (Morris et al. 2022).

References

Atwater BF, Hedel CW. 1976. Distribution of seed plants with respect to tide levels and water salinity in the natural tidal marshes of the northern San Francisco Bay estuary, California. US Geological Survey Menlo Park, California, USA.

De Smith MJ, Goodchild MJ, Longley PA. 2018. Univariate classification schemes in Geospatial Analysis-A Comprehensive Guide, 6th edn. The Winchelsea Press.

[DSC] Delta Stewardship Council. 2021a. Delta Adapts: Creating a Climate Resilient Future. Sacramento-San Joaquin River Delta Climate Change Vulnerability Assessment Draft Flood Hazard Assessment Technical Memorandum, June 2021. Sacramento, CA. Available from: https://www.deltacouncil.ca.gov/pdf/delta-plan/2021-06-17-flood-hazard-assessment-technical-memorandum.pdf

[DSC] Delta Stewardship Council. 2021b. Delta Adapts: Creating a Climate Resilient Future. Sacramento-San Joaquin Delta Climate Change Vulnerability Assessment, June 2021. Sacramento, CA.

[DSC] Delta Stewardship Council. 2022. Methods Used to Update Ecosystem Restoration Maps Using New Digital Elevation Model and Tidal Data. Appendix Q1 to the Delta Plan Amendments. Available from: https://deltacouncil.ca.gov/pdf/delta-plan/2022-06-29-appendix-q1-methods-used-to-update-ecosystem-restoration-maps-using-new-digital-elevation-model-and-tidal-data.pdf

Hester MW, Willis JM, Sloey TM. 2016. Field assessment of environmental factors constraining the development and expansion of Schoenoplectus californicus marsh at a California

tidal freshwater restoration site. Wetl Ecol Manag. 24:33–44. https://doi.org/10.1007/s11273-015-9448-9
Morris JT, Drexler J, Vaughn LS, Robinson A. 2022. An assessment of future tidal marsh resilience in the San Francisco Estuary through modeling and quantifiable metrics of sustainability. Front Environ Sci. 2384.
Morris JT, Renken KA. 2020. Past, present, and future nuisance flooding on the Charleston peninsula. PLOS ONE. 15:e0238770. https://doi.org/10.1371/journal.pone.0238770
Nerem RS, Beckley BD, Fasullo JT, Hamlington BD, Masters D, Mitchum GT. 2018. Climate-change–driven accelerated sea-level rise detected in the altimeter era. Proc Natl Acad Sci. 115:2022–2025. https://doi.org/10.1073/pnas.1717312115
[OPC] Ocean Protection Council. 2018. State of California Sea-Level Rise Guidance: 2018 Update. Ocean Prot Counc Sacram CA USA.
Schile LM, Callaway JC, Morris JT, Stralberg D, Parker VT, Kelly M. 2014. Modeling Tidal Marsh Distribution with Sea-Level Rise: Evaluating the Role of Vegetation, Sediment, and Upland Habitat in Marsh Resiliency. PLOS ONE. 9:e88760. https://doi.org/10.1371/journal.pone.0088760
[SFEI] San Francisco Estuary Institute. 2022. Landscape Scenario Planning Tool User Guide v. 2.0. Available from: https://www.sfei.org/documents/landscape-scenario-planning-tool-user-guide-v20

Appendix E to Managed wetlands for climate action: potential greenhouse gas and subsidence mitigation in the Sacramento-San Joaquin Delta

Modeling of subsidence with SUBCALC^2

Lydia J. S. Vaughn[1], Steven J. Deverel[2], Stephanie Panlasigui[1], Judith Z. Drexler[3], Marc A. Olds[2], Jose T. Diaz[2], Kendall Harris[1], James Morris[4], J. Letitia Grenier[1], April Robinson[1], Donna Ball[1]

[1]San Francisco Estuary Institute-Aquatic Science Center
[2]Hydrofocus, Inc.
[3]U.S. Geological Survey, California Water Science Center
[4]University of South Carolina

We estimated current and future subsidence and CO_2 flux for the entire Delta from 2017 to 2057 using the SUBCALC^2 model originally developed by Deverel and Leighton (2010) and updated in 2016 (Deverel et al. 2016). SUBCALC^2 uses Michaelis-Menten kinetics to simulate microbial oxidation within the organic and highly organic mineral soils. The primary inputs for the model include depth-to-groundwater, soil organic matter content above the water table, soil organic matter content below the water table, and thickness of the remaining peat.

SUBCALC^2 model equations, processes, and validation

SUBCALC^2 represents annual elevation change as the sum of four components:

$$S_T = S_o + S_c + S_w + S_B \quad (1)$$

where S_T =Total annual elevation change;

S_O = Elevation change due to microbial organic matter oxidation;

S_C = Elevation change due to consolidation as shown in equation 1;

S_W = Elevation change due to wind erosion; and

S_B = Elevation change due to burning.

Microbial oxidation

Elevation change due to microbial organic matter oxidation is represented as

$$S_O = \frac{omloss}{(\rho_B \times fom)} \quad (2)$$

where $omloss = cflux \times 2$;
$\rho_B = \rho_B$ =soil bulk density; and
fom =soil organic matter content.

We assumed that microbially mediated carbon loss or *clfux* follows Michaelis-Menten kinetics and the rate of oxidation is limited by the soil organic matter content (Browder and Volk, 1978):

$$clfux = \frac{(clfuxmax \times st)}{Km+st} \quad (3)$$

where:
cflux= gaseous carbon loss from the soil in grams cm^{-2} yr^{-1} due to microbial oxidation;
cfluxmax = maximum gaseous carbon loss from the soil in grams cm^{-2} yr^{-1};
Km = Michealis-Menten constant; and
st = total carbon substrate in the soil above the water table in grams of carbon.

Initially, the organic and mineral masses were calculated for the simulation depth (*simdpth)* as follows:

$$mass = simdpth \times \rho_B ;$$
$$ommass = mass \times fom ;$$
$$minmass = mass \times (1 - fom) ; \text{ and}$$
$$st = \sum(\frac{fom_i}{2} \times \rho_{Bi}) \times simdpth_i$$

for each segment of the soil profile i within the total simulation depth $simdpth$,

where:
$mass$ =total soil mass;
$ommass$ =mass of organic matter in the simulation depth (*simdpth*); and
$minmass$ = mineral mass in the simulation depth.

The simulation depth is assumed to be the depth of organic soil above the water table and encompasses the entire unsaturated zone.

We approximated the relationship between microbial oxidation of organic carbon and soil organic carbon content from carbon flux data from Sherman Twitchell Island (Deverel and Leighton, 2010; Hemes et al., 2019), Bouldin Island (Hemes et al., 2019), Sherman Island (Knox et al., 2015), and Staten Island. We fit the measured fluxes with the associated total soil substrate in the footprint of each eddy measurement site by adjusting the Michaelis-Menten constant (*Km*) in equation 3. We fit a linear regression relating *Km* with the estimated substrate mass to derive the following equation used to calculate *Km* for the initial total soil substrate.

$$Km = (-4.2732 \times st) + 51.709 \quad (4)$$

Figure A4. Measured carbon fluxes and estimated soil substrate with fitted SUBCALC[2] results.

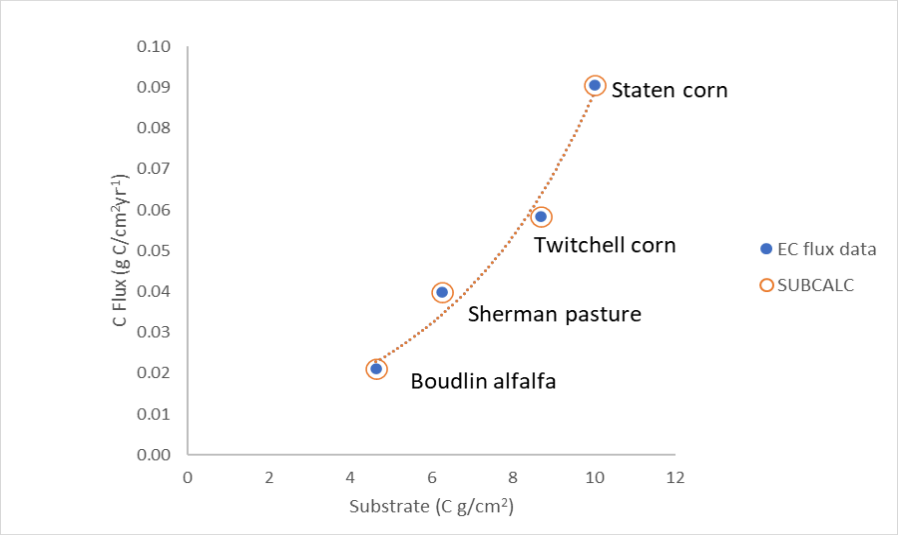

Figure A5. Fitted SUBCALC[2] relationship for Michaelis-Menten constant (*Km*) and total substrate.

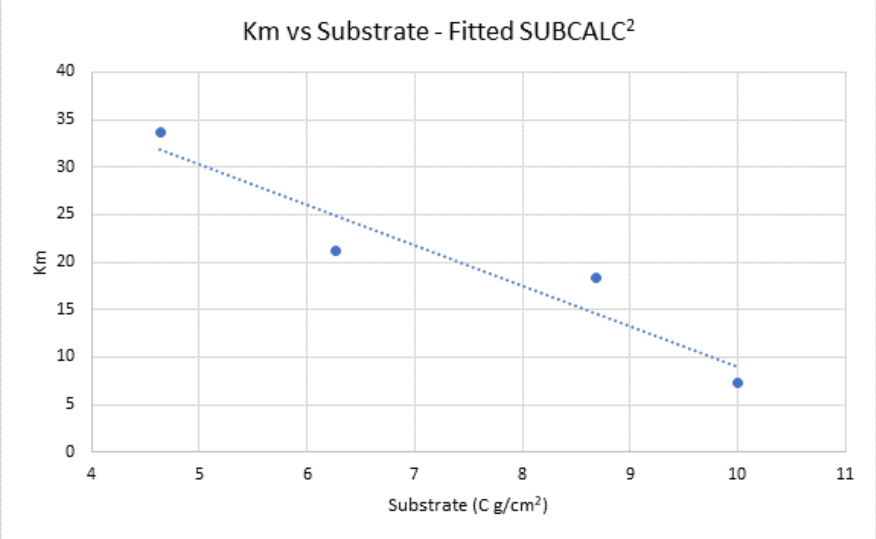

Consolidation

The model estimates subsidence due to consolidation, S_c, using Terzaghi's principle of effective pressure (Terzaghi, 1925). We used the Vega et al. (1984) expression for consolidation within a small increment of pressure change due to dewatering in a soil column of thickness *d* (expressed in cm) as:

$$S_c = m_v \times d \times \Delta p \quad (5)$$

Where S_c is the subsidence due to consolidation in cm;
m_v is the coefficient of volume compressibility in cm^{-1}; and
Δp is the change in pressure (cm).

We estimated consolidation of organic deposits and m_v from extensometer data from Twitchell Island as described in Deverel and Leighton (2010). Using the Twitchell Island data we estimated an m_v value of 0.00156 cm^{-1}. Based on data presented in Drexler et al. (2009) that shows relatively higher bulk density below the oxidized zone on farmed islands relative to adjacent non-farmed remnant channel islands, we assumed the upper 150 cm was subject to compaction. We used this coefficient of volume compressibility value and equation B5 to estimate annual compaction due to lowering of the depth to groundwater. We assumed that the Δp term in equation B5 was equal to the annual change in subsidence due to oxidation, wind erosion and burning as drainage ditches have been deepened to compensate for these decreases in elevation. Therefore,

$$\Delta_p = S_o + S_w + S_b \quad \text{(B6)}$$

Wind erosion and burning

Easterly spring winds cause erosion of organic soils (Schultz and Carlton, 1959; Schultz et al., 1963), with most or all the wind-eroded soil from bare asparagus fields. The California Department of Water Resources (CDWR 1980) reported wind-erosion soil losses from 0.6 to 3 cm per year. Carlton and Schultz (1966) estimated 0.57 inch (1.44 cm) per year of wind erosion on Terminous Tract from 1927 to 1957. We specified 1.44 cm per year of wind erosion where asparagus was grown or where the land was fallow based on the Carlton and Schultz (1966) data because it is the only known documentation of wind erosion measurements. Development of a wind erosion model is difficult due to lack of historic wind data. We determined the historical land use for Bacon Island, Lower Jones Tract and Mildred Island from Rojstaczer et al. (1991). Corn generally replaced asparagus and other vegetable crops in the Delta in the 1960s, and the model calculated minimal wind erosion after 1970 except for Bacon Island, where asparagus was grown into the early 1990s.

Weir (1950) and Cosby (1941) stated that farmers burned peat soils to control weeds and diseases once every 5 to 10 years and 7.6 to 12.7 cm (3 to 5 inches) of peat disappeared during a single burning. Farmers burned more frequently during World War II (Weir, 1950; Rojstaczer et al., 1991). From 1926 to 1941 on Bacon Island, Mildred Island and Lower Jones Tract, we specified 1.7 cm per year of burning. As per Weir (1950), we assumed that burning annually rotated among individual fields and a yearly soil loss would adequately represent average conditions during this period. During 1941–1945, we specified 2.54 cm of soil loss per year. Alan Carlton (former University of California Extension Specialist, personal communication, 1997) stated that farmers generally did not burn organic soils intentionally after the 1950s. The data from Weir (1950) were used because they were the only available data for soil loss due to burning. Moreover, two sources indicate similar rates: Weir (1950) and Cosby (1941). Burning and wind erosion were deemed negligible for present-day conditions.

For each annual time step, S_O, S_W, S_B, and S_C were calculated based on newly calculated mass of organic matter (*ommass*), fom and ρ_B:

$$ommass_t = ommass_{t-1} - omflux_{t-1} - S_{B't-1} \times \rho_{B't-1} \times fom_{t-1} - S_{W't-1} \times \rho_{B't-1} \times fom_{t-1} + S_{T't-1} xfom_{und} \times \rho_{B,u} + S_{T't-1} xfom_{und} \times \rho_{B,und} \quad (7)$$

where subscripts t and t-1 denote the current and previous annual time steps; fom_{und} = fraction organic matter for material beneath the water table; and $\rho_{B,und}$ = bulk density for material beneath the water table.

The *fom* for the current time step was calculated by dividing the *ommass* for the current time step (equation B6) by the total mass (*ommass+minmass*). The new bulk density was calculated by dividing the total mass by the simulation depth (*simdpth)*. Underlying fraction organic matter and bulk density were specified based on data presented in Drexler et al. (2009) where:

$$\rho_{B,und} = -0.21 \ln ln (fom \times 100) + 1.01 \quad (8)$$

Soil temperature effect

Deverel and Rojstaczer (1996) showed that the logarithm of soil carbon loss was significantly correlated with soil temperature. We estimated future soil temperature increases in the delta region based on soil moisture and temperature modeling from Bradford et al. (2019). Bradford et al. (2019) projected mean annual soil temperature at 50 cm for western North America for 2010 to 2050 and 2070 to 2100. They based the temperature and soil moisture projections on both the Representative Concentration Pathway (RCP) 4.5 (intermediate) and RCP 8.5 (worst-case) climate models. The average soil temperature within the legal Delta was projected to increase to 17.67ºC (RCP 4.5) and 17.96ºC (RCP 8.5), which are average increases of 1.12ºC and 1.41ºC from 2010, respectively. By 2100, average soil temperatures in the Delta were projected to reach 18.72ºC (RCP 4.5) and 20.40ºC (RCP 8.5). This represents a total increase of 2.17ºC and 3.85ºC from 2010, respectively. To determine the cumulative temperature change for a given period, the SUBCALC[2] model uses the linear interpolation of the projected temperature increases from Bradford et al. (2019).

For estimating temperature effects on future oxidative subsidence rates and carbon flux, we used a relationship for temperature and respiration rate based on work by Van't Hoff as described in Lloyd and Taylor (1994). We used an empirical value of 1.94 for Q_{10} from Deverel and Rojstaczer (1996). The change in flux for each year is dependent on the cumulative change in temperature from the first year and the initial flux (*clflux*$_0$) when *deltc* = 0. The change in flux is then added to the calculated flux from equation 3 as follows.

$$log_{10} k = a + bT$$
$$R = k_R M = Ae^{BT}$$
$$B = \frac{ln(Q_{10})}{10}$$

The soil temperature effect is modeled as:

$$delcflux = (cflux_0 \times e^{\frac{\ln ln\, Q_{10}}{10} \times deltc}) - cflux_0 \quad \text{(B12)}$$

where:
deltc = change in temperature from first year;
delcflux = cumulative change in flux from the first year;
$cflux_0$ = initial carbon flux from the first year; and
Q_{10} = 1.94 (Deverel & Rojstaczer, 1996)

We used linear interpolation of the average of the data provided by Bradford et al. (2019) within the Delta for the two segments 2010-2050 and 2050-2099 to determine the predicted temperature for the year. The model parameter *rcp* determines which temperature model from Bradford et al. (2019) to use for the simulation.

Application of SUBCALC^2 to future scenarios

We created geospatial layers with the distribution of each major input parameter which we then intersected to generate a grid of model inputs. The output results consisted of three-dimensional stacked rasters where each "layer" represented each year in the simulation. Both the intersected input grids and output rasters have a 90-ft (27.432 m) resolution.

Depth-to-Groundwater (DTW)

We applied SUBCALC^2 to areas where the peat soils are drained for most of the year. In areas used for rice cultivation or permanently flooded wetlands where the DTW is at land surface, SUBCALC^2 returns no value for subsidence or CO_2 flux as these land uses effectively stop soil oxidation and subsidence. We estimated the average annual DTW for seasonal wetlands and areas too wet for agriculture described in Deverel et al. (2015) as 60 cm. We estimated the DTW for all other areas in the Delta based on data from the Soil Survey Geographic Database (SSURGO), monitoring wells, drain measurements, and experience from local landowners and field personnel. The DTW values used are shown in Figure A6.

Peat Thickness

We estimated the current remaining peat thickness and extent based on work done by Deverel and Leighton (2010) to determine the peat bottom elevation. Deverel and Leighton (2010) analyzed data from more than 1,100 borings within the Delta and used geostatistical methods to generate an interpolated peat bottom elevation layer. Using this layer, we estimated the remaining peat thickness by subtracting the land surface elevations from the 2017 LiDAR survey (CDWR, 2019). Where the peat has thinned such that the water table is below the bottom of the peat, the SUBCALC^2 model assumes that no additional organic matter is added from underneath. Where the peat has effectively vanished, SUBCALC^2 assumes there is no subsidence and that the CO_2 flux rate is dependent on the land use (crop).

Figure A6. Estimated present day depth-to-groundwater in meters.

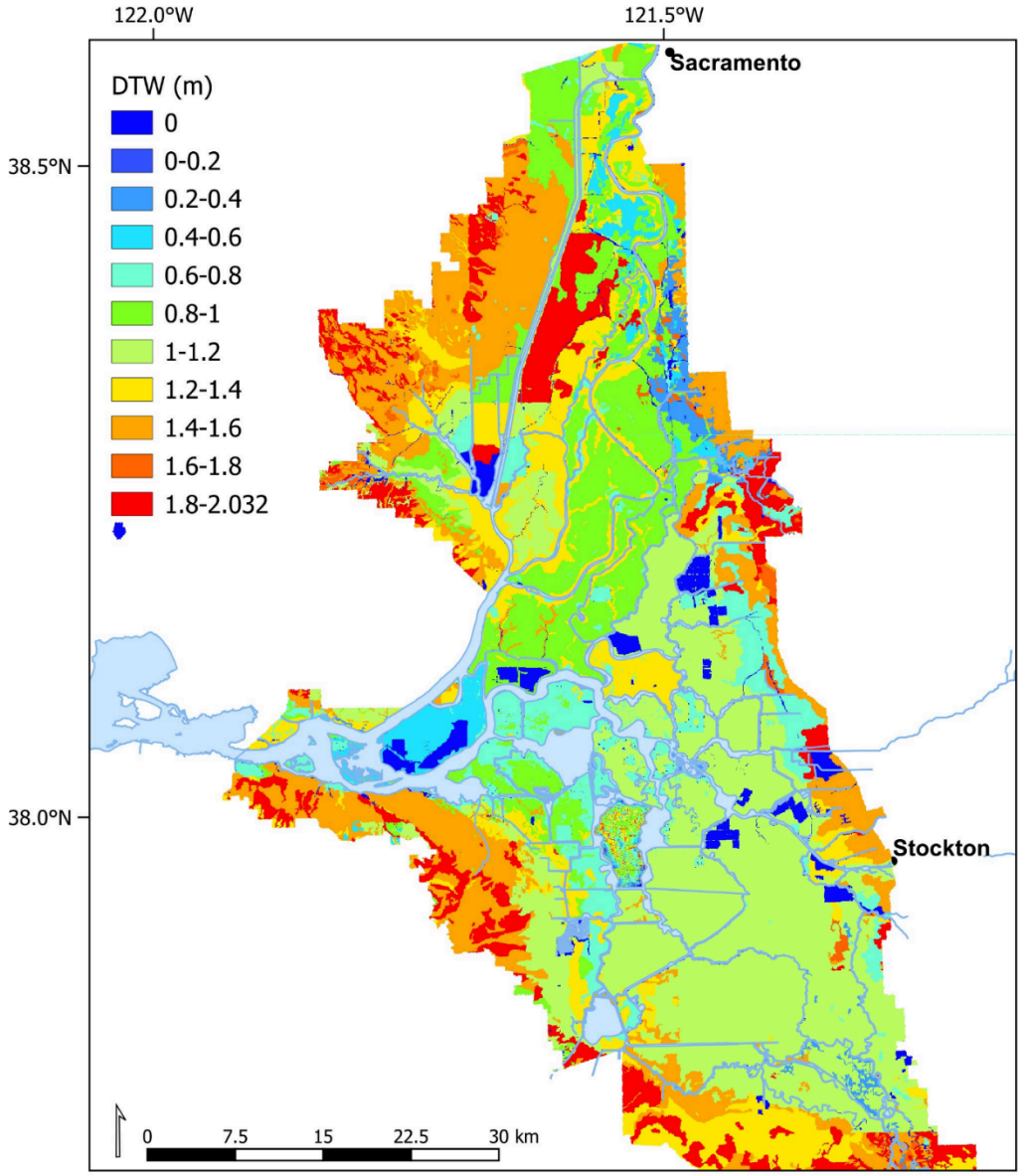

Soil Organic Matter

We estimated soil organic matter content in both the unsaturated (above the water table) and saturated zones from the soil map units in the SSURGO database (SSURGO). We determined which soil map units were composed of organic and highly organic mineral soils and reviewed the ranges of soil organic matter content in the typical profiles for each map unit. Figure A7 shows the mapped extent of each organic and highly organic mineral soil map unit within the Delta and the extent of the peat deposits as mapped by Deverel and Leighton (2010). For the unsaturated zone, we calculated the weighted average of the median organic matter value for each horizon within approximately 1 meter from the soil surface, a typical value for DTW (Fig. A6). We adjusted these values using an empirical relationship between the median SSURGO organic matter and measured organic matter from samples taken on Delta islands (Figure A8). This relationship was originally developed by Deverel et al. (2016) using soil organic matter

samples collected from Bacon and Sherman Islands (Deverel and Leighton 2010), Twitchell Island (Deverel et al. 2016), and Staten Island (Deverel et al. 2017). The relationship was updated in this report using additional data collected on Staten Island in 2020. In the saturated zone, we used the maximum organic matter value reported in SSURGO for the horizon immediately below the last horizon used for the unsaturated zone. This value represents the organic matter content of the soil that may be dewatered each year as drains are deepened to keep up with subsidence.

Figure A7. SSURGO organic and highly organic mineral soil map units. The estimated remaining peat extent is shown as a dashed line based on mapping presented in Deverel et al.(2016).

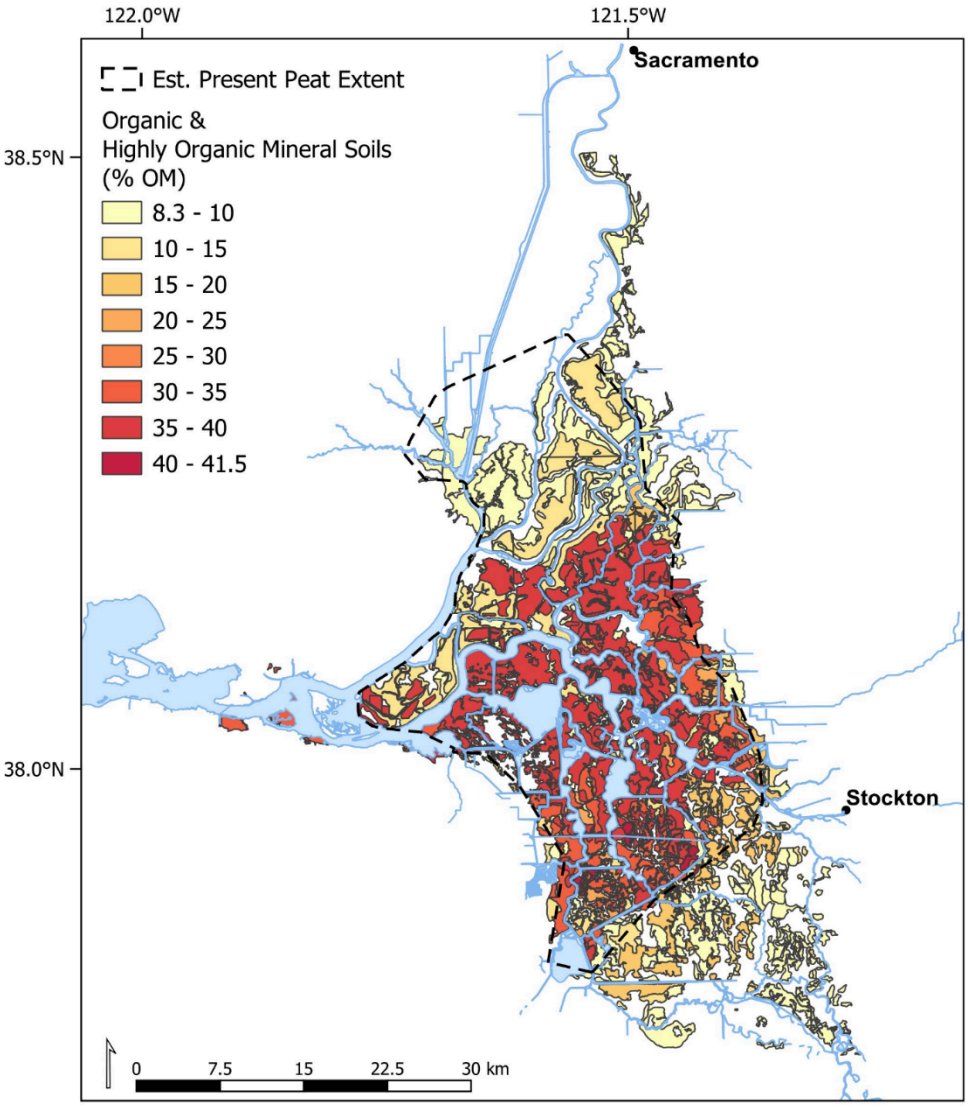

Figure A8. Relationship between average measured surface organic matter and median SSURGO organic matter; updated from Deverel et al. (2016) with additional data collected from Staten Island in 2020.

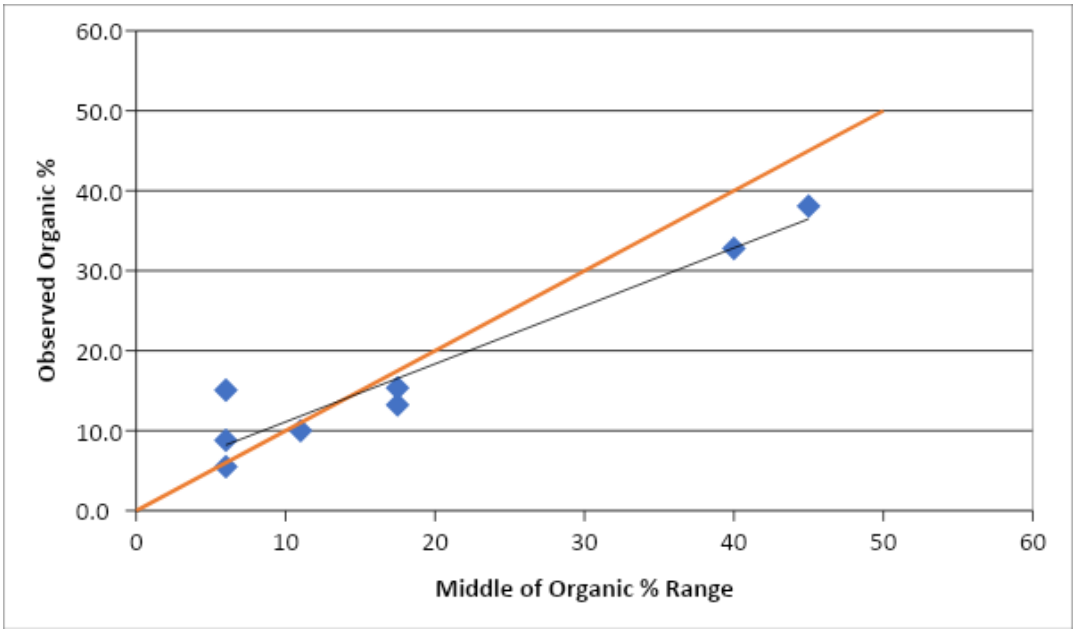

References

Bradford, J. B., Schlaepfer, D. R., Lauenroth, W. K., Palmquist, K. A., Chambers, J. C., Maestas, J. D., & Campbell, S. B., 2019. Climate-driven shifts in soil temperature and moisture regimes suggest opportunities to enhance assessments of dryland resilience and resistance. *Frontiers in Ecology and Evolution*, *7*(SEP).

Browder, J.A. and Volk, B.G., 1978, Systems model of carbon transformations in soil subsidence, Ecological Modeling 5, 269 – 292.

Carlton, A.B. and Schultz, H.B., 1966, Annual Statements of Progress for Project 1686, 1955 to 1966, Peat land conservation and peat dust abatement, University of California, College of Agriculture, Agricultural Experiment Station, Department of Soils and Plant Nutrition, Davis, California

[CDWR] California Department of Water Resources, 1980, Subsidence of organic soils in the Sacramento-San Joaquin Delta, Central District, Sacramento, California.

[CDWR] California Department of Water Resources, 2019, 2017 Delta LiDAR Dataset. [accessed 2020 Apr 30] Available at: http://gisarchive.cnra.ca.gov/iso/ImageryBaseMapsLandCover/LIDAR/DeltaLIDAR2017/

Cosby, S.W., 1941, Soil survey of the Sacramento-San Joaquin Delta Area, California: Bureau of Plant Industry, U. S. Department of Agriculture, p. 1-47.

Deverel S, Jacobs P, Lucero C, Dore S, Kelsey TR. 2017. Implications for Greenhouse Gas Emission Reductions and Economics of a Changing Agricultural Mosaic in the Sacramento–San Joaquin Delta. San Franc Estuary Watershed Sci. [accessed 2021 September 20];15:. https://doi.org/10.15447/sfews.2017v15iss3art2

Deverel SJ, Ingrum T, Leighton D. 2016. Present-day oxidative subsidence of organic soils and mitigation in the Sacramento-San Joaquin Delta, California, USA. *Hydrogeology Journal*, *24*(3), 569–586

Deverel SJ, Leighton DA. 2010. Historic, Recent, and Future Subsidence, Sacramento-San Joaquin Delta, California, USA. San Franc Estuary Watershed Sci. [accessed 2019 November 12];8:. https://doi.org/10.15447/sfews.2010v8iss2art1

Deverel SJ, Rojstaczer S. 1996. Subsidence of agricultural lands in the Sacramento-San Joaquin Delta, California: Role of aqueous and gaseous carbon fluxes. Water Resour Res. 32:2359–2367.

Drexler JZ, Fontaine CS, Deverel SJ. 2009b. The legacy of wetland drainage on the remaining peat in the Sacramento — San Joaquin Delta, California, USA. Wetlands. 29:372–386. https://doi.org/10.1672/08-97.1

Hemes KS, Chamberlain SD, Eichelmann E, Anthony T, Valach A, Kasak K, Szutu D, Verfaillie J, Silver WL, Baldocchi DD. 2019. Assessing the carbon and climate benefit of restoring degraded agricultural peat soils to managed wetlands. Agric For Meteorol. 268:202–214. https://doi.org/10.1016/j.agrformet.2019.01.017

Knox SH, Sturtevant C, Matthes JH, Koteen L, Verfaillie J, Baldocchi D. 2015. Agricultural peatland restoration: effects of land-use change on greenhouse gas (CO2 and CH4) fluxes in the Sacramento-San Joaquin Delta. Glob Change Biol. 21:750–765. https://doi.org/10.1111/gcb.12745

Lloyd J. and Taylor JA. 1994. On the temperature dependence of soil respiration. *Functional ecology*, pp.315-323.

Rojstaczer SA, Hamon RE, Deverel SJ, Massey CA. 1991. Evaluation of selected data to assess the causes of subsidence in the Sacramento-San Joaquin Delta, California, U.S. Geological Survey Open File Report 91-193. [Also available at: https://doi.org/10.3133/ofr91193]

Schultz HB, Carlton AB, Lory F. 1963. Interpolating methods for wind erosion protection in San Joaquin asparagus, *California Agriculture* 17(9):4-5. https://calag.ucanr.edu/archive/?article=ca.v017n09p4

Schultz HB, Carlton, AB. 1959. Field windbreaks for row crops, *California Agriculture* 13(11):5-6https://calag.ucanr.edu/archive/?article=ca.v013n11p5

[SSURGO] Soil Survey Staff, Natural Resources Conservation Service, United States Department of Agriculture. Soil Survey Geographic (SSURGO) Database.

Terzaghi K. 1925. Principles of soil mechanics. IV: settlement and consolidation of clay. Engineering News Record, vol 95. McGraw–Hill, New York

Vega, G. F., Yamamota, S, and Helm, D.C., 1984, Techniques for prediction of subsidence in Poland, J.F. (ed.) Guidebook to studies of land subsidence due to ground-water withdrawal, United Nations Educational, Scientific and Cultural Organization (UNESCO), American Geophysical Union, Book Crafters, Chelsea, Michigan

Weir, W.W., 1950, Subsidence of peat lands of the Sacramento-San Joaquin Delta, California, Hilgardia, v. 20, p.27-56.

Appendix F to Managed wetlands for climate action: potential greenhouse gas and subsidence mitigation in the Sacramento-San Joaquin Delta

Modeling of accretion in managed nontidal peat-building wetlands with SEDCALC

Lydia J. S. Vaughn[1], Steven J. Deverel[2], Stephanie Panlasigui[1], Judith Z. Drexler[3], Marc A. Olds[2], Jose T. Diaz[2], Kendall Harris[1], James Morris[4], J. Letitia Grenier[1], April Robinson[1], Donna Ball[1]

[1]San Francisco Estuary Institute-Aquatic Science Center
[2]Hydrofocus, Inc.
[3]U.S. Geological Survey, California Water Science Center
[4]University of South Carolina

Potential accretion time series were simulated using the SEDCALC model (Deverel et al. 2014), which was calibrated based on the Twitchell Island impounded wetlands subsidence-reversal demonstration project. The SEDCALC model was originally developed by (Callaway et al. 1996) and adapted by Deverel et al. (2014) to integrate data and simulate Delta managed nontidal marsh vertical accretion. Deverel et al. (2014) presented the following description of SEDCALC:

> *Potential accretion time series were simulated using SEDCALC. The Callaway et al. (1996) model simulates surface organic matter and mineral deposition, subsurface organic matter decomposition, below-ground organic matter production and consolidation, and movement of mineral and organic matter accumulated at the surface to older age classes. The model also calculates changes in cohort composition, mass, and porosity, and tracks the depth and elevation of the cohort in the accumulating sediment. Model inputs include surface organic matter and mineral inputs to the marsh, rates of organic matter decomposition, below-ground organic matter production and consolidation, initial and limiting porosities, sea level rise and organic and mineral particle densities.*

Deverel et al. (2014) modified the Callaway et al. (1996) model to accept time-varying inputs for first- decomposition rates, organic and mineral inputs, initial and final porosity, and subsidence rates. Deverel et al. (2014) calibrated SEDCALC using data for age, porosity, bulk density and organic-matter content from cores collected from Franks Tract State Recreation Area (Drexler et al. 2009a, 2009b) and the Twitchell Island demonstration project (Miller et al. 2008).

Model calibration and validation

For this simulation, Sedimentation-Erosion-Table data for the Twitchell Island West Pond from 1996 – 2018 was utilized to calibrate and validate the model (Fig. A9). Using the inputs for the

first 20 years for the Twitchell Island West Pond wetland, we simulated accretion from 2018 to 2100. SEDCALC inputs are presented in Tables A6 and A7.

Figure A9. Measured and simulated accretion in the Twitchell Island West Pond, 1996 – 2018. Time-varying inputs for SEDCALC are initial porosity (h2oin), limiting porosity (porelim) surface mineral matter deposition (minin), and surface organic matter deposition (orgin). Inputs with constant values through all the simulation are percent refractory organic matter (refract), below-ground organic matter production (undpro), decomposition rate constant (k_{decomp}), consolidation constant (k_{cons}), organic particle density (orgden), and mineral particle density (minden). SEDCALC inputs are presented in Tables A6 and A7.

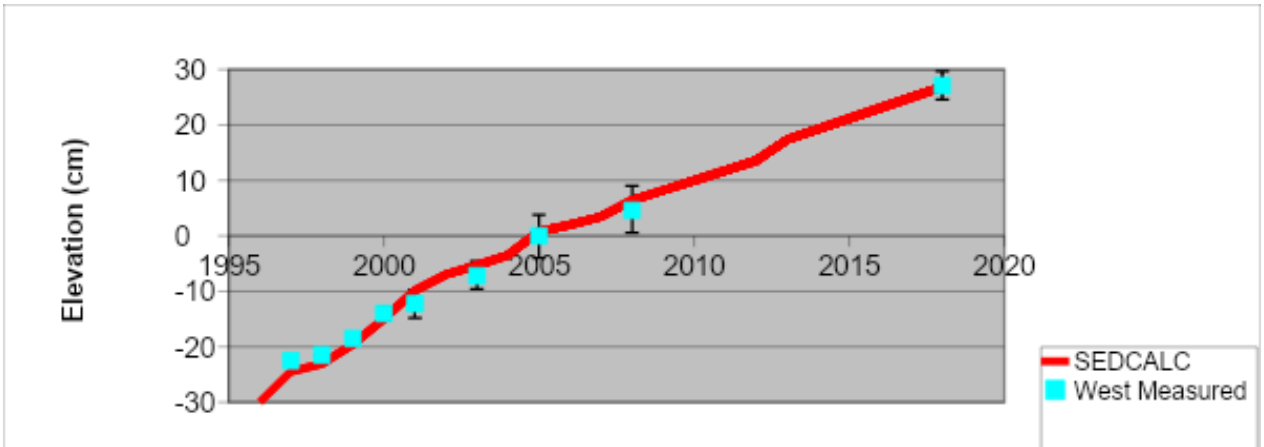

The first assumption is that impounded wetlands will be flooded to a constant depth of about 25 cm throughout the simulation. In other words, as wetlands accrete, weirs will be raised concomitantly to keep the ponding depth constant. The second assumption is that plant community composition and colonization, residence time, mineral input, and consolidation dynamics will be homogeneous throughout the Delta and similar to those observed in the Twitchell Island demonstration project. The third assumption is that mineral sediments input will have the same magnitude observed in Twitchell Island, and will remain constant over time.

Model inputs

Time-varying inputs for SEDCALC are initial porosity (h2oin), limiting porosity (porelim) surface mineral matter deposition (minin), and surface organic matter deposition (orgin). Inputs with constant values through all the simulation are percent refractory organic matter (refract), below-ground organic matter production (undpro), decomposition rate constant (k_{decomp}), consolidation constant (k_{cons}), organic particle density (orgden), and mineral particle density (minden). SEDCALC inputs are presented in Tables A6 and A7.

Table A6. SEDCALC inputs constant through simulation

Parameter	Value
refract	0.4
undpro (g cm^{-2})	0.06
k_{decomp} (yr^{-1})	0.41

k_{cops}	2.5
orgden (g cm^{-2})	1.14
minden (g cm^{-2})	2.61

Table A7. Time-varying SEDCALC inputs

Year	h2oin	porelim	minin (g cm-2)	orgin (g cm^{-2})
2018	0.82	0.93	0.20	0.22
2019	0.83	0.93	0.20	0.22
2020	0.85	0.93	0.60	0.11
2021	0.89	0.93	0.60	0.11
2022	0.91	0.93	0.20	0.11
2023	0.90	0.93	0.20	0.11
2024	0.88	0.92	0.08	0.11
2025	0.88	0.92	0.03	0.11
2026	0.94	0.92	0.03	0.11
2027	0.95	0.93	0.03	0.11
2028	0.96	0.93	0.03	0.11
2029	0.98	0.93	0.03	0.11
2030	0.98	0.93	0.03	0.11
2031	0.98	0.93	0.03	0.11
2032	0.98	0.93	0.03	0.11
2033	0.98	0.95	0.03	0.11
2034	0.98	0.95	0.03	0.11
2035	0.98	0.95	0.03	0.11
2036	0.98	0.95	0.03	0.11
2037	0.98	0.95	0.03	0.11
2038	0.98	0.95	0.03	0.11
2039	0.98	0.94	0.03	0.11
2040	0.98	0.95	0.03	0.11
2041	0.98	0.95	0.03	0.11
2042	0.98	0.94	0.03	0.11
2043	0.98	0.94	0.03	0.11
2044	0.98	0.94	0.03	0.11
2045	0.98	0.95	0.03	0.11
2046	0.98	0.95	0.03	0.11
2047	0.98	0.95	0.03	0.11
2048	0.98	0.95	0.03	0.11
2049	0.98	0.95	0.03	0.11

Year	h2oin	porelim	minin (g cm-2)	orgin (g cm^{-2})
2050	0.98	0.95	0.03	0.11
2051	0.98	0.95	0.03	0.11
2052	0.98	0.95	0.03	0.11
2053	0.98	0.95	0.03	0.11
2054	0.98	0.95	0.03	0.11
2055	0.98	0.95	0.03	0.11
2056	0.98	0.95	0.03	0.11
2057	0.98	0.95	0.03	0.11
2058	0.98	0.95	0.03	0.11
2059	0.98	0.95	0.03	0.11
2060	0.98	0.95	0.03	0.11
2061	0.98	0.95	0.03	0.11
2062	0.98	0.95	0.03	0.11
2063	0.98	0.95	0.03	0.11
2064	0.98	0.95	0.03	0.11
2065	0.98	0.95	0.03	0.11
2066	0.98	0.95	0.03	0.11
2067	0.98	0.95	0.03	0.11
2068	0.98	0.95	0.03	0.11
2069	0.98	0.95	0.03	0.11
2070	0.98	0.95	0.03	0.11
2071	0.98	0.95	0.03	0.11
2072	0.98	0.95	0.03	0.11
2073	0.98	0.95	0.03	0.11
2074	0.98	0.95	0.03	0.11
2075	0.98	0.95	0.03	0.11
2076	0.98	0.95	0.03	0.11
2077	0.98	0.95	0.03	0.11
2078	0.98	0.95	0.03	0.11
2079	0.98	0.95	0.03	0.11
2080	0.98	0.95	0.03	0.11
2081	0.98	0.95	0.03	0.11
2082	0.98	0.95	0.03	0.11
2083	0.98	0.95	0.03	0.11
2084	0.98	0.95	0.03	0.11
2085	0.98	0.95	0.03	0.11
2086	0.98	0.95	0.03	0.11
2087	0.98	0.95	0.03	0.11
2088	0.98	0.95	0.03	0.11

Year	h2oin	porelim	minin (g cm-2)	orgin (g cm^{-2})
2089	0.98	0.95	0.03	0.11
2090	0.98	0.95	0.03	0.11
2091	0.98	0.95	0.03	0.11
2092	0.98	0.95	0.03	0.11
2093	0.98	0.95	0.03	0.11
2094	0.98	0.95	0.03	0.11
2095	0.98	0.95	0.03	0.11
2096	0.98	0.95	0.03	0.11
2097	0.98	0.95	0.03	0.11
2098	0.98	0.95	0.03	0.11
2099	0.98	0.95	0.03	0.11
2100	0.98	0.95	0.03	0.11

Application of SEDCALC to future scenarios

The potential for subsidence reversal and carbon sequestration through impounded wetlands implementation was estimated for the Delta from 2018 to 2100. Locations in the Delta where surface elevation in 2017 is below the mean sea level (MSL) in 2017 were deemed suitable for impounded wetlands implementation. The DEM and MSL in 2017 are presented in Figure A10. Resulting locations where the 2017 MTL is greater than the 2017 surface elevations is presented in Figure A11. The analysis was done at a 10-m resolution.

Figure A10. Land surface elevation and mean sea level from 2017 tidally referenced digital elevation model (DEM) (DSC 2022; SFEI 2022)

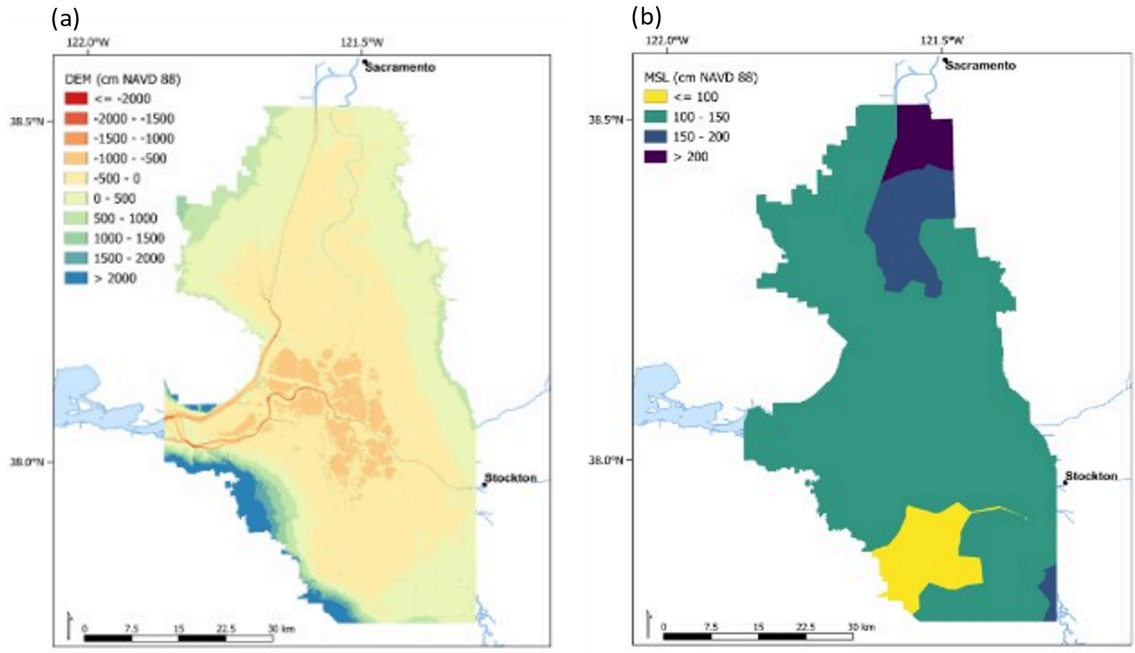

Figure A11. Area deemed suitable for impounded wetlands implementation, based on mean sea level (MSL) and surface elevation. Hashed area indicates where surface elevations (DEM) are below MSL.

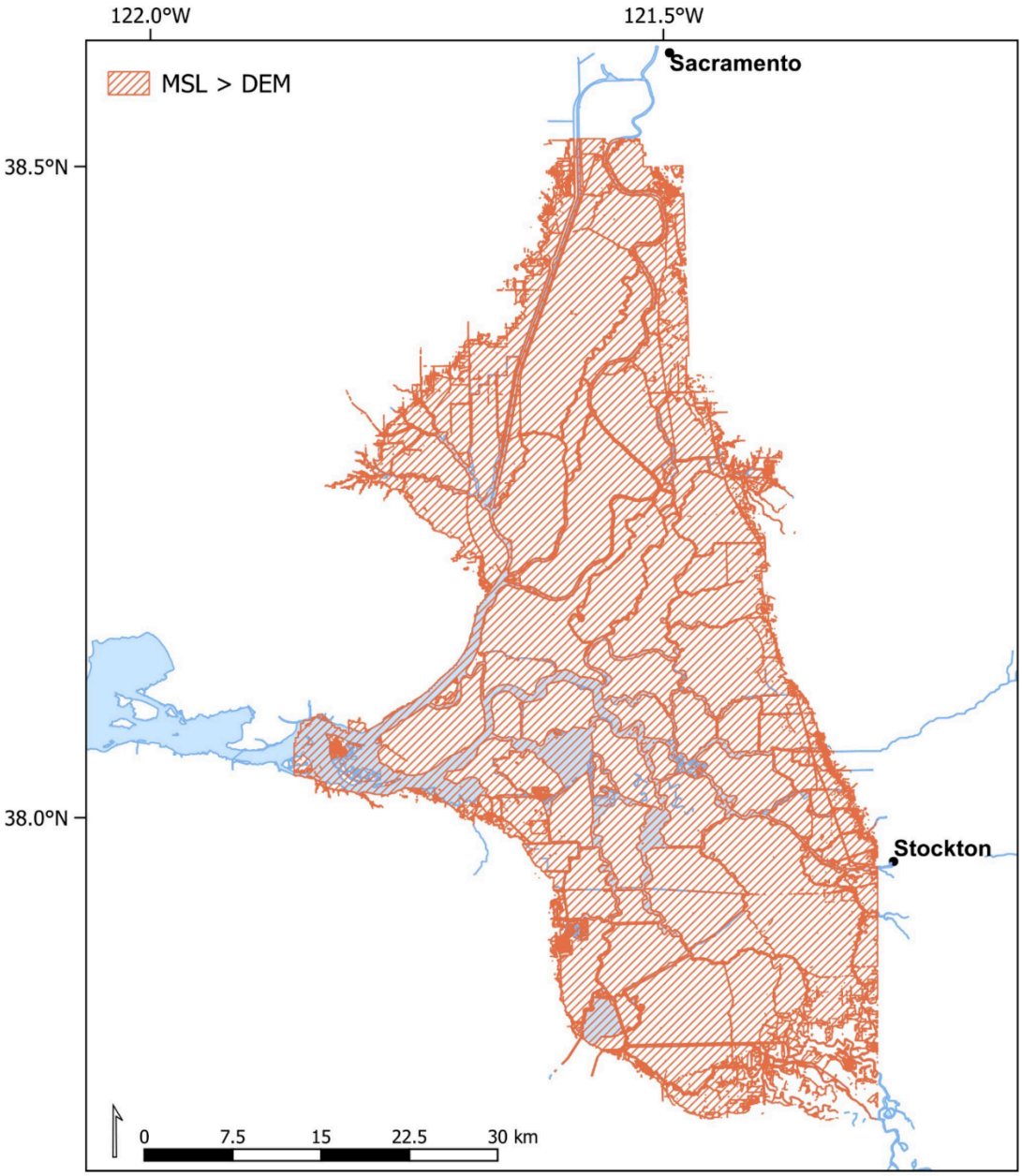

SEDCALC ran from 2018 to 2100. SEDCALC cumulative accretion time series are presented in Figure A12, while cumulative carbon uptake timeseries are presented in Figure A13.

Figure A12. SEDCALC simulated cumulative accretion from 2010 to 2100.

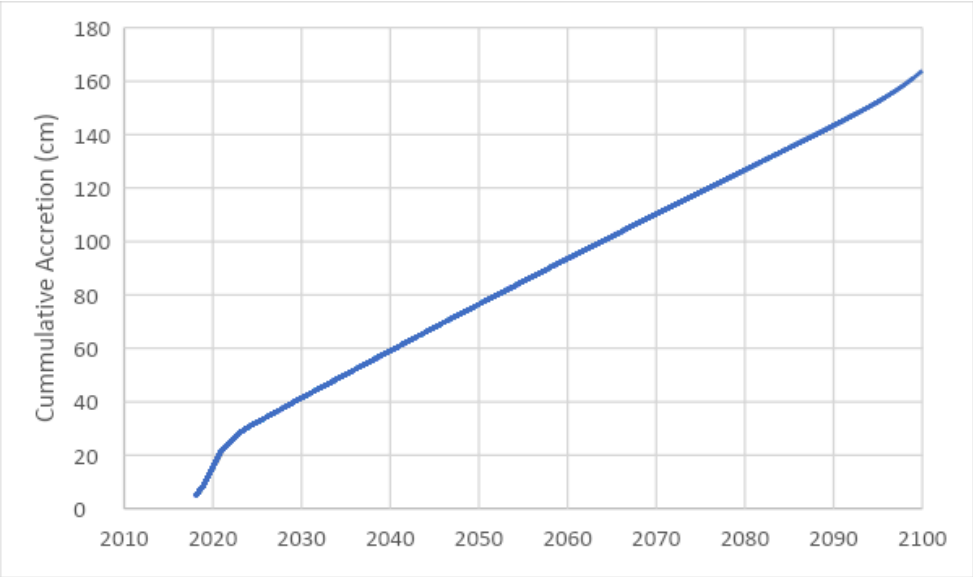

Figure A13. SEDCALC cumulative carbon uptake from 2010 to 2100.

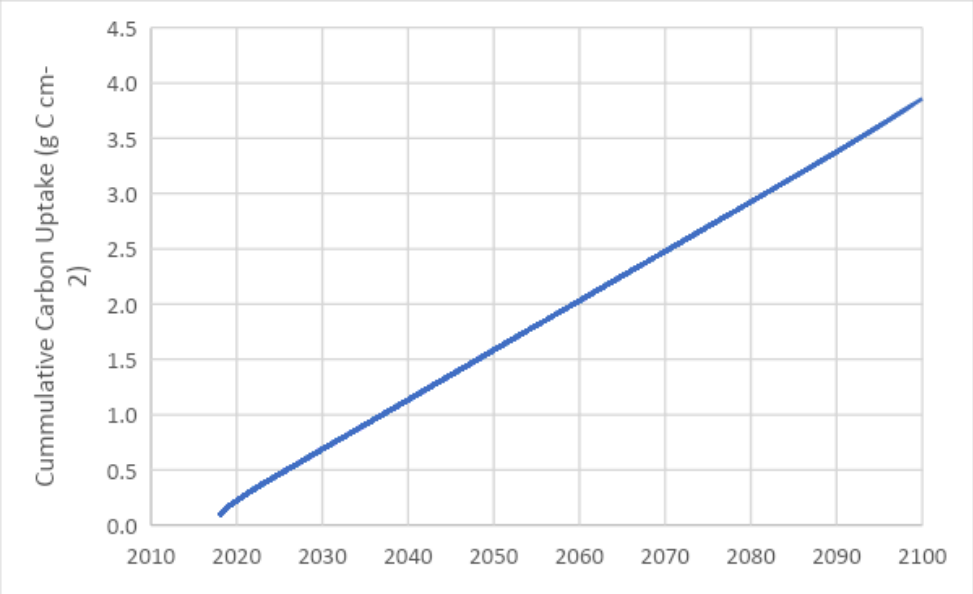

To incorporate SLR into the model, the domain was classified into two areas based on hydrological and geomorphological criteria for each SLR scenario. SLR scenarios of 1.1 ft by 2060 and 2.6 ft by 2060 were considered. The two domains for 1.1 ft SLR by 2060 are presented in Figure A3b. SLR timeseries used for the two domains are presented in Table A5. As a result, MSL is calculated for every year and model cell using the following formula:

$$MSL_{i,\,j,\,t,k} = MSL^{0}_{i,\,j} + SLR_{i,\,j,\,t,k} \quad (1)$$

Where:
$MSL_{i,\,j,\,t,k}$: mean sea level for row i, column j, year t, and SLR scenario k
$MSL^{0}_{i,\,j}$: mean sea level in 2017 for row i and column j
$SLR_{i,\,j,\,t,k}$: sea level rise between 2017 and year t for row i, column j, and SLR scenario k

In areas of the Delta where potential accretion is larger than the difference between MSL and and the initial elevation, impounded wetlands accretion is assumed to stop once the surface elevation catches up with the tidal datum. As a result, effective accretion is less or equal than potential accretion, and is calculated using the following formula:

$$Acc^{eff}_{i,j,t,k} = min(Acc^{pot}_{t},\ MSL_{i,\,j,\,t,k} - DEM_{i,\,j,\,t,k}) \quad (2)$$

Where:

$Acc^{eff}_{i,j,t,k}$: Effective accretion for row i, column j, year t, and SLR scenario k

Acc^{pot}_{t}: Potential accretion for year t obtained from SEDCALC

$DEM_{i,\,j,\,t,k}$: Surface elevation for row i, column j, year t, and SLR scenario k

Then, surface elevation is updated with accretion for the following year:

$$DEM_{i,\,j,\,t+1,k} = DEM_{i,\,j,\,t,k} + Acc^{eff}_{i,j,t,k} \quad (3)$$

Similarly, carbon uptake is calculated as a fraction of the potential carbon uptake, proportional to the effective accretion value.

$$C^{eff}_{i,j,t,k} = min(C^{pot}_{t},\ \frac{Acc^{eff}_{i,j,t,k}}{Acc^{pot}_{t}} * C^{pot}_{t})$$

Where:

$C^{eff}_{i,j,t,k}$: Effective carbon sequestration for row i, column j, year t, and SLR scenario k

C^{pot}_{t}: Potential carbon sequestration obtained from SEDCALC for year t

An important source of uncertainty in SEDCALC accretion estimates is “[the] extent to which accreting sediment will consolidate as it transforms from loose and highly porous material

collected from the Twitchell Island impounded marsh to consolidated peat soil …" (Deverel et al. 2014). The main variables that control consolidation are k_{cons} and porelim. While k_{cons} controls the speed of consolidation, porelim represents the limiting porosity. To quantify the uncertainty in accretion estimates, Deverel et al. (2014) varied k_{cons} and porelim, as presented in Table A6 and Figure A14.

Table A6. Sensitivity of years to reach 2014 sea level as a function of porelim and k_{cons}. Adapted from (Deverel et al. (2014)

Simulation number	k_{cons} value	porelim (as a fraction)	Years to reach 2014 sea level on Twitchell Island
11	10	0.94	202
12	100	0.94	130
13	100	0.925	156
14	10	0.925	257
15	250[a]	0.94	106
16	250	0.925	117

a. Maximum value from (Callaway et al. (1996)

Figure A14. Deverel et al. (2014) estimated vertical accretion for Twitchell impounded marsh, east pond. Values posted with each curve are model inputs for k_{cons} and porelim (separated by a backslash) shown in Table A6. Adapted from Deverel et al. (2014).

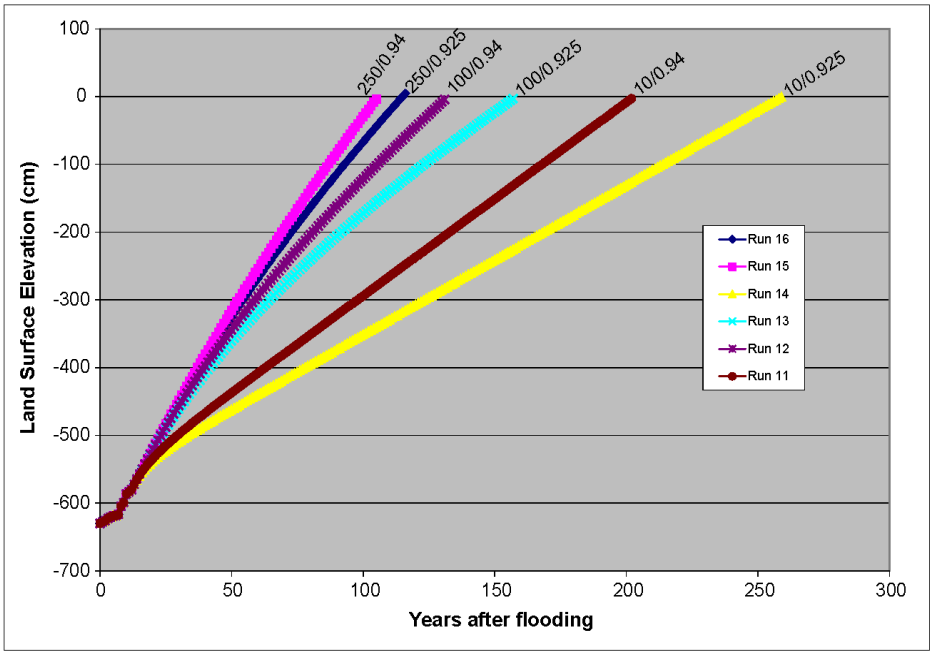

References

Callaway J, Nyman J, Delaune R. 1996. Sediment accretion in coastal wetlands: A review and a simulation model of processes. Curr Top Wetl Biogeochem. 2:2–23.

Deverel SJ, Ingrum T, Lucero C, Drexler JZ. 2014. Impounded marshes on subsided islands:: Simulated vertical accretion, processes, and effects, Sacramento-San Joaquin Delta, CA USA. San Fr Estuary Watershed Sci. 12:1–23. https://doi.org/10.15447/sfews.2014v12iss2art5

Drexler JZ, de Fontaine CS, Brown TA. 2009a. Peat Accretion Histories During the Past 6,000 Years in Marshes of the Sacramento-San Joaquin Delta, CA, USA. Estuaries Coasts Port Repub. 32:871–892. http://dx.doi.org.libproxy.berkeley.edu/10.1007/s12237-009-9202-8

Drexler JZ, Fontaine CS, Deverel SJ. 2009b. The legacy of wetland drainage on the remaining peat in the Sacramento — San Joaquin Delta, California, USA. Wetlands. 29:372–386. https://doi.org/10.1672/08-97.1

[DSC] Delta Stewardship Council. 2022. Methods Used to Update Ecosystem Restoration Maps Using New Digital Elevation Model and Tidal Data. Appendix Q1 to the Delta Plan Amendments. Available from: https://deltacouncil.ca.gov/pdf/delta-plan/2022-06-29-appendix-q1-methods-used-to-update-ecosystem-restoration-maps-using-new-digital-elevation-model-and-tidal-data.pdf

Miller R, Fram MS, Fujii R, Wheeler G. 2008. Subsidence Reversal in a Re-Established Wetland in the Sacramento-San Joaquin Delta, California, USA. San Fr Estuary Watershed Sci. 6:. https://doi.org/10.15447/sfews.2008v6iss3art1

[SFEI] San Francisco Estuary Institute. 2022. Landscape Scenario Planning Tool User Guide v. 2.0. Available from: https://www.sfei.org/documents/landscape-scenario-planning-tool-user-guide-v20

Appendix G to Managed wetlands for climate action: potential greenhouse gas and subsidence mitigation in the Sacramento-San Joaquin Delta

Supplemental maps

Lydia J. S. Vaughn[1], Steven J. Deverel[2], Stephanie Panlasigui[1], Judith Z. Drexler[3], Marc A. Olds[2], Jose T. Diaz[2], Kendall Harris[1], James Morris[4], J. Letitia Grenier[1], April Robinson[1], Donna Ball[1]

[1]San Francisco Estuary Institute-Aquatic Science Center
[2]Hydrofocus, Inc.
[3]U.S. Geological Survey, California Water Science Center
[4]University of South Carolina

Figure A15. Estimated present-day net greenhouse gas (GHG) emissions from model analysis of the *Modern* scenario

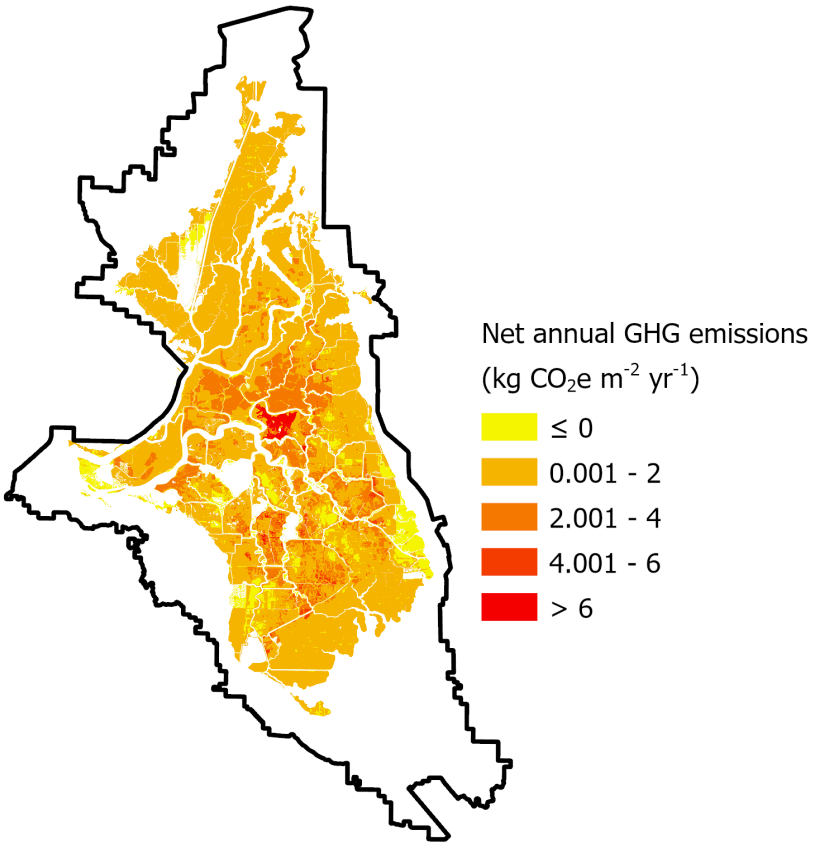

Figure A16. Difference in elevation between the *Maximum potential* and *Reference* scenario at the end of 40-year simulation period. Positive numbers indicate a gain in elevation relative to reference conditions.